

The influence of subaquatic springs in lacustrine sedimentation: origin and paleoenvironmental significance of homogenites in karstic Lake Banyoles (NE Spain)

Mario Morellón^{*1, 2}, Flavio S. Anselmetti^{3, 2}, Blas Valero-Garcés⁴, Santiago Giral⁵, Daniel Ariztegui⁶, Alberto Sáez⁷, M. Pilar Mata⁸, Fernando Barreiro-Lostres⁴, Mayte Rico⁴, Ana Moreno⁴

¹ *Instituto de Geociencias (CSIC, UCM), Calle José Antonio Nováis, 2, 3ª planta, 3b. Facultad de Ciencias Geológicas, Univ. Complutense. 28040 Madrid, Spain.*

² *Swiss Federal Institute of Aquatic Science and Technology, Eawag, Ueberlandstrasse 133, CH-8600 Dübendorf, Switzerland.*

³ *Institute of Geological Sciences and Oeschger Centre of Climate Change Research, University of Bern. Baltzerstrasse 1. CH-3012 Bern, Switzerland.*

⁴ *Department of Environmental Processes and Global Change. Pyrenean Institute of Ecology (IPE) – CSIC. Campus de Aula Dei. Avda Montañana 1005. E-50059 Zaragoza, Spain.*

⁵ *Institute of Earth Sciences Jaume Almera (ICTJA-CSIC). Carrer Lluís Solé i Sabarís s/n. E-08028 Barcelona, Spain.*

⁶ *Section of Earth Sciences. University of Geneva. Rue des Maraîchers 13. CH-1205 Genève, Switzerland.*

⁷ *Department of Stratigraphy, Paleontology and Marine Geosciences. Universitat de Barcelona. C/ Marti Franques s/n. E-08028 Barcelona, Spain.*

⁸ *Instituto Geológico y Minero de España (IGME). C/ Calera 1. E-28760 Tres Cantos (Madrid), Spain.*

*Corresponding author. E-mail address: mario.morellon@igeo.ucm-csic.es

ABSTRACT

Banyoles (42°08'N, 2°45'E) is the largest and deepest lake of karstic-tectonic origin in the Iberian Peninsula. The lake comprises two basins and six sub-circularly shaped sub-basins fed by subaqueous springs. Periods of intense groundwater inflow in the deepest sub-basins lead to the fluidization and re-suspension of previously deposited sediments and subsequent settling forming homogenite deposits on the southern basin intermediate platforms. The multiproxy analysis of sediment cores combined with high resolution seismic stratigraphy (3.5 KHz pinger and multi-frequency Chirp surveys), allows a precise reconstruction of depositional environments and related hydrological variability and groundwater inflow during the last ca. 7.6 cal kyrs BP. According to the age model based on $^{137}\text{Cs}/^{210}\text{Pb}$ and AMS ^{14}C dating, homogenite deposition occurred between 7.2 and 5.5 cal kyrs BP, stopped during the middle Holocene (5.5 - 2.8 cal kyrs BP) and greatly increased during the last two millennia with a total of 17 homogenite layers up to 75 cm-thick. The onset of this unique sedimentation mode ca. 3 cal kyrs BP coincides with an increase in lake level, evidenced by the onlapping of fine-grained, distal sediments over coarser massive, carbonate-rich, littoral deposits. A detailed, multidisciplinary study of the homogenites (sedimentology, physical properties, high-resolution elemental geochemistry, mineral composition, grain-size, organic matter content and SEM) combined with seismic stratigraphy demonstrates that the fluidization events triggering the formation of the homogenites were caused by higher and more intense local groundwater inflow, related to increased rainfall during the Late Holocene and likely intensified by land use changes during the last millennia.

Keywords: karstic lake, subaquatic springs, groundwater, turbidity plumes, homogenites, Holocene

1. Introduction

Groundwater constitutes an essential hydrological resource in Mediterranean areas characterized by a summer drought period and frequent negative hydrological balance phases, which are particularly threatened by global change (García-Ruiz et al., 2011; Younger et al., 2002). In these regions, aquifers are essential for sustaining human activities and limnic ecosystems, (Álvarez-Cobelas et al., 2005; Edmunds et al., 2004; Shapley et al., 2005). The groundwater input to the hydrological balance is rarely quantified in most lakes, however, subaqueous springs are commonly identified as a significant source for groundwater in lake systems (Assayag et al., 2008; Canals et al., 1990; Colomer et al., 2002; Matter et al., 2010). Recently, such springs and associated pockmarks have been described and imaged thanks to high-resolution geophysical and limnological surveys (e.g., Lake Ohrid, (Matter et al., 2010), Lake Kivu (Ross et al., in review)). In spite of their variable relative importance in the hydrological balance of these systems, subaquatic springs commonly supply cool and oxygenated waters, rich in ions and nutrients, leading to the establishment of particular subenvironments and specific habitats for endemic species within lake systems (Descy et al., 2012a; Matter et al., 2010).

Ecological and limnological responses to subaquatic springs are well-studied (e.g., Dead Sea (Ionescu et al., 2012), Lake Bogoria (Dadheech et al., 2013), Lake Kivu (Descy et al., 2012b)) and extensive research has been carried out on associated carbonate sedimentary features (i.e., microbialites, tepee structures, diagenetic iron-rich shoreline indicators and carbonate crusts) (Burne and Moore, 1987; Rosen et al., 2004; Rosen et al., 2002; Warren, 1982; Winter, 1999). However, less attention has been paid to the physical effects of groundwater input in sedimentation and its potential to remobilize significant amounts of sediments (Bloesch, 1995; Draganits and Janda, 2003). Examples of fluidization and resuspension of offshore lake sediments and consequent re-deposition of thick ‘homogeneous’

layers have been exclusively described as a result of shaking and/or sub-aqueous mass-wasting slope processes caused by earthquakes (Beck, 2009). However, intense and focused groundwater input through subaquatic springs could be also able to produce a similar effect in sedimentation, not yet described in detail in lake settings. Although these groundwater-fed lake basins often provide long, continuous sequences with high temporal resolutions, suitable for palaeohydrological and palaeoclimate reconstructions (Morellón et al., 2009; Valero-Garcés et al., 2013), an adequate understanding of sedimentary processes is essential to reconstruct the evolution of groundwater inputs, their impact in lake sedimentation and their role in homogenite formation (Shapley et al., 2005).

Lake Banyoles (NE Spain) belongs to a groundwater-fed karstic system and constitutes a unique example in the Iberian Peninsula of offshore sedimentation partly controlled by the activity of sub-aqueous springs. Geophysical and limnological surveys during the last decades have documented the resuspension and fluidization of sediments by focused groundwater inflow at the deepest sub-basins of the lake (Canals et al., 1990; Casamitjana and Roget, 1993), leading to the development of turbidity plumes (Serra et al., 2005). These ‘fluidization events’ have been related with episodes of intense rainfall in the recharge area of the aquifer feeding the lake (Soler et al., 2009; Soler et al., 2007). Although Banyoles has been extensively investigated from a limnological point of view, the impact of groundwater dynamics on the sediments across the lake, and the spatial and temporal extent of this impact at longer timescales than the last few decades, remains unknown. Moreover, the depositional history of the lake has been exclusively studied at the littoral areas of the sedimentary basin (Cho Martínez, 2012; Höbig et al., 2012; Pérez-Obiol and Julià, 1994; Valero-Garcés et al., 1998) and at emerged pre-Holocene paleolake deposits (Julià-Brugués, 1977; Leroy, 1997; Løvlie and Leroy, 1995).

This paper aims to fill this gap in the investigations carried out in Banyoles and provides a Holocene sedimentary reconstruction using offshore sediments with special emphasis on sedimentary processes associated with fluidization events related to higher groundwater input episodes through subaquatic springs. The combined use of high-resolution seismic stratigraphy and a multi-proxy analysis of sediment cores recovered at offshore areas of the lake enable a precise reconstruction of the spatial extent, timing and different intensity of groundwater discharge. The associated sedimentary processes are evaluated in relation to climate variability and changes in land use during the last millennia.

2. Regional setting

2.1 Geological and geomorphological setting

Lake Banyoles (42°1'N; 2°4'E, 173 m a.s.l.), located in the NE margin of the Iberian Peninsula, 20 km west of the Mediterranean Sea (Fig. 1A) lies in a tectonic-karstic basin (Julià, 1980) and is formed by several cone-like karstic depressions (Fig. 1B). The lake is located in the eastern South-Pyrenean Foreland Basin (Bischoff et al., 1994; Burbank et al., 1992) affected by widespread Neogene extension (Saula et al., 1994; Tassone et al., 1994). The bedrock comprises the mid Eocene Banyoles Formation, mainly composed of marine, organic- and pyrite-rich marls and mudstones, underlain by the Eocene Beuda Formation consisting of massive gypsum (200-300 m), and the 100 to 200 m thick Perafita Formation dolostones (Barnolas, 1992; Mató i Palós et al., 1996; Serra-Kiel et al., 2003). The contact between these last two formations has led to a bedrock 'de-dolomitization' process due to gypsum dissolution, a particularly intense karstification mechanism responsible for the formation and collapse of the Lake Banyoles depressions (Bischoff et al., 1994). Karstic processes (e.g., collapse depressions, intermittent springs, karren fields) are still active in the lake catchment (Canals et al., 1990; Julià, 1980; Sanz, 1981), as demonstrated by the

12/11/1978 collapse, when a new sub-basin ('Estanyol Nou') was formed near to the southwestern shore (Höbig et al., 2012).

Lake Banyoles is the last remnant of a larger lacustrine basin developed during Pliocene-Quaternary times, known as the Banyoles-Besalú system, which occupied 90 km² (Canals et al., 1990; Julià-Brugués, 1977). Travertine formations and calcareous lithologies are common, both in ancient terraces (Julia Bruguès and Suc, 1980; Leroy, 1997) and present lacustrine deposits (Coma et al., 1988; Coma et al., 1987). The age of the travertine formation damming the eastern margin of the modern lake is ~120 to 45 ka BP (Julià and Bischoff, 1991), which represents the potential maximum age of the lacustrine deposits accumulated within the basin.

The littoral zone of the modern lake (0-3 m water depth) is covered by a thin macrophyte vegetation belt of *Phragmites*, *Schoenoplectus* and *Myriophyllum*. Sediments range from travertines and calcareous sands in the littoral areas, to carbonate-rich silts and clays in the distal areas (Rieradevall and Roca, 1995).

2.2 Morphometry, hydrology and limnology of the lake

The lake has a N-S elongated shape and a surface of 118 Ha. The lake is formed by 7 main circular-shaped sub-basins (B1 to B6), with steep margins and water depths ranging from 7.5 to 44 m, connected by shallower, flat platforms (ca. 20 m and 5-10 m water depths in the southern and northern areas, respectively) (Canals et al., 1990; Moreno-Amich and García-Berthou, 1989) (Fig. 1B). Karstic depressions confer a lobed shape to the lake shoreline, and a shallow (< 12 m maximum water depth) and narrow (< 500 m) sill in the center divides the lake in two basins, here referred as northern and southern ones (Fig. 1B).

The lake is hydrologically open and mainly groundwater-fed through subaqueous springs located in the deepest sub-basins of the southern basin (B1 and B2) (Canals et al.,

1990; Moreno-Amich and García-Berthou, 1989). Surface water input derived from the 11.42 km² catchment drained by the creeks located in the western area of the lake has been quantified as 100 to 300 l/s for May-September 1984, whereas output through the canals at the eastern margin (Fig. 1C) ranges from 568 to 1080 l/s for the same period (Canals et al., 1990; Dutras et al., 1986). Thus, groundwater supplies 85% of the total water input (Casamitjana et al., 2006). Lake water in southern basin is characterized by a lower residence time and higher oxygenation levels than water in the northern lobe. Particularly, sub-basin B1 provides 90% of groundwater input (Serra et al., 2005). The other main sub-basins of the northern basin (Fig. 1B) have a lower groundwater input so that anoxic conditions and sulfide production at the hypolimnion occur (Garcia-Gil et al., 1993; Guerrero et al., 1978). Thus, the 6 sub-basins are connected by their epilimnetic waters, but their respective hypolimnions are isolated and show differential anoxic periods, ranging from 1 to 12 months/year (Prat and Rieradevall, 1995).

Surface lake waters are sulphate and calcium-rich ($[\text{SO}_4^{2-}] > [\text{HCO}_3^{2-}] > [\text{Ca}^{2+}] > [\text{Mg}^{2+}]$) (Bischoff et al., 1994), with an electrical conductivity of 1300 to 1400 $\mu\text{S}/\text{cm}$ and a pH between 7 and 8.1 (MAGRAMA, 2006). Water temperature is highly variable, ranging from 8 to 25 °C depending on the water depth and season (Rieradevall and Roca, 1995). Oxygenation conditions are also spatially variable and depending of groundwater input, ranging from oxic (0-7 m water depth), to one month of anoxia (sub-basin B1 > 12 m water depth), and to long-lasting anoxia (sub-basins B3 and B4, > 12 m) (Rieradevall and Roca, 1995). The lake is monomictic, with water stratification from April to October. A chemocline is also present in sub-basins B1 and B4 at 19-20 and 13-17 m water depth respectively, which leads to long anoxic periods in the hypolimnion (Rieradevall and Roca, 1995).

Differences in the thermal inertia and incoming flux through the subaqueous springs, located in the northern and southern basins, move denser water during the winter season from

the shallower northern to the deeper southern basin. This leads to a bottom current with a flow of 20000 l/s and a velocity of up 12 cm/s that redistributes water between the two basins, replacing northern basin waters every ~5 days. This exchange constitutes the main current dominating circulation in the lake (Casamitjana et al., 2006; Roget et al., 1993).

2.3 Groundwater and turbidity plumes

The lake constitutes a ‘trop-plein’ of a complex aquifer system whose recharge area is located in the Alta Garrotxa Range, 15 to 40 km northwards (Brusi et al., 1990; Sanz, 1981). The NE-SW trending Albanyà fault, east of the lake, constitutes a subvertical dam for the groundwater (Moreno-Amich and García-Berthou, 1989). Most of the deepest sub-basins (B1, B2, B4, B5 and B6) are filled with several meters of sediments maintained in suspension by the intense groundwater inflows forming a sharp and horizontal, upper sediment interface, known as the lutocline which is recognizable in seismic profiles (Fig. 1D) (Canals et al., 1990). These suspensions have particle concentrations varying from 0.18 to $< 10^{-3}$ g/l and rather constant temperatures (~19°C) (Casamitjana et al., 2006). According to geophysical surveys and sedimentological analyses, sediments in B1, B3 and B4 appear as ‘mobile’ particles in suspension, whereas they are usually denser and more consolidated in B2, resulting in an acoustic bedding at the bottom of this sub-basin (Colomer et al., 2002). The momentum of the underground spring and sediment grain-size determines the maximum height that the lutocline can rise to in each case (Casamitjana et al., 1996; Colomer et al., 1998). Fluctuations of the lutocline depths in B1, B3 and B4 are comparatively smaller than B2 and show consistent shifts (Casamitjana and Roget, 1993).

Most intense fluidization and re-suspension processes, and associated hydrothermal plumes, are restricted to the deepest sub-basins B1 and B2. Sub-basin B1 is fed by the largest groundwater flow (~500 l/s). Its sediment fill has a vertical thickness of 45 to 50 m and a

sediment density of 100 to 130 g/l (Colomer et al., 2002). Its lutocline oscillates from 29.2 to 32.0 m water depth (Serra et al., 2005) (Fig. 1D). In contrast, B2 experiences periodical large fluctuations in sediment density from 280 to 180 g/l and larger lutocline migrations (from 25 to 45 m). Sediment fluidization processes occurs episodically associated with particular intense rainfall events in the aquifer recharge area (average monthly values 1.5 to 4.5 times larger than the long term mean (1970-1999) (Colomer et al., 2002). Thus, sub-basin B2 acts as an overflow of the groundwater system.

Due to the difference between temperature of the lutocline and the hypolimnetic water immediately above B1, an upward-directed permanent hydrothermal plume develops (Colomer et al., 2001). This plume carries a suspension of particles from the lutocline up to a maximum height, which varies depending on the stratification depth of the water column. During the mixing period, this plume reaches the surface of the lake, spreading laterally and forming a ~7 m-thick turbidity current, with a sediment concentration of ~0.01 g/l (Serra et al., 2005). According to sediment-trap studies, particle fluxes oscillate from 10 to 25 g m⁻² day⁻¹ near to B1 to < 5 g m⁻² day⁻¹ in more distant areas of the southern basin (Serra et al., 2002; Serra et al., 2005).

An additional temporal, hydrothermal turbidity plume develops above sub-basin B2 due to fluidization events after intense rainfall in the aquifer recharge area (Soler et al., 2009). The onset of the fluidization is characterized by episodic ground-water influx entering through preferential paths in the more consolidated sediment at the bottom of sub-basin B2. The water pressure through small diameter conducts within the sediment causes a high mean upward velocity, which is three orders of magnitude greater than in perennial plume B1. After such an event, water-flux velocity decreases progressively and resuspends the settled sediment. Finally, when sediments are totally fluidized, the episodic hydrothermal plume of sub-basin B2 resembles that of the perennial plume of B1 (Soler et al., 2009). When the

hydrothermal plume in sub-basin B2 is fully developed, a large quantity of sediment is transported upwards from the lutocline, resulting in an increase in sedimentation rates in the southern basin (ca. $156 \text{ g m}^{-2} \text{ day}^{-1}$), which is one order of magnitude higher than in periods without fluidization, when only the B1 hydrothermal plume remains active (Casamitjana et al., 2006; Serra et al., 2002; Soler et al., 2009).

As both basins of the lake (N and S) are separated by a shallow sill (Fig. 1B), sediments transported by turbidity plumes are restricted during the stratification period to the southern one. In contrast, during the mixing period, particles can reach the surface of the lake, spreading laterally and subsequently settling across the entire lake bottom (Soler et al., 2009). However, sedimentation in the northern basin is not significantly affected by re-suspended sediments and carbonate-rich silts and sands with abundant encrusted charophyte stems and other calcitic bioclasts (e.g., ostracods, gastropods) are predominant (Serra et al., 2005). Thus, the effect of turbidity plumes on sedimentation is mostly restricted to the southern basin.

3. Materials and methods

A geophysical survey was carried out in April 2011 using a high-resolution, single-channel seismic system with a centre frequency of 3.5 kHz (GeoAcoustic pinger source) and a EdgeTech Chirp 3100-P multi-frequency profiler, covering 22 km and 14 km of seismic lines, respectively. This dense grid consisting of ~36 km of seismic lines provides a mean spatial resolution of ~100 m between each line (Fig. 1C). Seismic processing workshop software was used for the processing of the pinger data (bandpass filter, flat gain) and the resulting seismic data set was interpreted using the Kingdom Suite software.

In May 2011, three pairs of overlapping sediment cores (BAN-11-1A, 2A and 3A) with maximum lengths of ~13, 12 and 5 m, respectively, were recovered using an Uwitec© percussion coring equipment installed on a floating raft. This research focuses on core 1A,

recovered in the flat platform between sub-basins B1 and B2, at ca. 21 m water depth. Additional coring sites 2A and 3A are located in the northernmost area of the lake and sub-basin B3, respectively. Three short, gravity cores were obtained to recover the uppermost part and the sediment/water interface of the three sequences. Seven additional short cores (BAN-12-1, 2, 3, 4, 5, 6 and 8) were recovered in July 2012 along a transect between B1, B2 and the location of the longest core BAN-11-1A (Fig. 1C). Cores recovering suspended sediments of sub-basins B1 and B2 (BAN-12-1 and 2) were maintained in upright position until sediments were stable and settled down, before excess water was eliminated. The uppermost 60 cm of the BAN-11-1A sequence was sub-sampled in the field every 1 cm for ^{137}Cs and ^{210}Pb dating.

Physical properties (magnetic susceptibility, gamma density, P-wave velocity) were measured in core BAN-11-1A with a Geotek Multi-Sensor Core Logger (MSCL) every 1 cm. All the cores were subsequently split in two halves and imaged with a digital camera. The Lightness (L^*) parameter was obtained from the core pictures using Adobe Photoshop CS and Image J software. Lithotypes were defined after visual and microscopic smear slides observation, applying the methodology described in (Schnurrenberger et al., 2003) (Table 1).

Elemental composition of core BAN-11-1A sediments was obtained by using an AVAATECH XRF core scanner at a resolution of 5 mm and under two different working conditions: i) with an X-ray current of 0.8 mA, at 10 s count time and 10 kV X-ray voltage for the measurement of Al, Si, P, S, Cl, Ar, K, Ca, Ti, V, Cr, Mn and Fe; and ii) with an X-ray current of 2 mA, at 30 s count time and 30 kV X-ray voltage for the measurement of Ni, Cu, Zn, Ga, Ge, As, Se, Br, Rb, Sr, Y, Zr, Nb, Au, Pb, Th and U. The XRF results are expressed as counts per second (cps) and only chemical elements with mean cps over 1500 were considered to be statistically significant.

Grain size of short cores BAN-12-1 and 2 was measured every 4 cm. Core BAN-11-1A was measured at variable resolutions: for grain size: ~8 cm at the uppermost 610 cm and

~25 cm at the lowermost part of the sequence, for TOC and TIC every 3 cm, and for X-ray diffraction every 9 cm. Grain size was determined using a Malvern Mastersizer 2000. Samples were pre-treated with 15% hydrogen peroxide in a hot plate at 80°C to eliminate the organic matter; a dispersant agent and ultrasound treatment were used prior to measurement. Total organic carbon (TOC) and total inorganic carbon (TIC) were measured with a LECO SC 144 DR elemental analyzer. Whole sediment mineralogy was characterized by X-ray diffraction with a Bruker-AXS D5005 (working conditions: Cu α , 40 kV, 30 mA and graphite monochromator) and relative mineral abundance was determined using peak intensity following the procedures described in (Chung, 1974a; Chung, 1974b). Results are expressed in percentages with respect of the total dry weight of the sample.

Scanning electron microscope images were taken at dried sediment samples of cores BAN-11-1A, BAN-12-1 and -2 under low-vacuum conditions in an environmental scanning electron microscope FEI Inspect on uncoated fragmented samples. Backscattered electron (BSE) images were obtained in order to detect compositional differences of the components as grey level contrast. In addition, energy dispersive X-ray spectrometry (EDS) analysis was performed when necessary.

The chronology of the lake sequence is based on: i) 9 Accelerator Mass Spectrometry (AMS) ^{14}C dates from core BAN-11-1A, analyzed at the ETH-Zürich Laboratory of Ion Beam Physics and at DirectAMS radiocarbon services (Seattle, USA) (Table 2) and on ii) $^{137}\text{Cs}/^{210}\text{Pb}$ dating by gamma spectroscopy at Eawag (Dübendorf, Switzerland). Excess (unsupported) ^{210}Pb was calculated as difference between total ^{210}Pb and ^{226}Ra for individual samples. Corrected radiocarbon dates were converted into calendar years BP with Calib 6.0 software using the INTCAL 09 calibration curve (Reimer et al., 2009), selecting the median of the 95.4% distribution (2σ probability interval) (Table 2). The age-depth relationship was

constructed by linear interpolation of the 1963 AD ^{137}Cs maximum activity peak and calibrated radiocarbon dates using Analyseries (Paillard et al., 1996).

4. Results

4.1 Seismic Stratigraphy

In spite of frequent gas masking throughout the lake basin, locally high penetration into the sub-surface down to the acoustic basement allowed tracking of the bedrock morphology in many parts of the lake. Maximum seismic penetration up to 20 m in the northern basin of the lake (Fig. 1D), where gas masking is more frequent, and 18 m in the southern basin (Fig. 2) did not reach the substratum. These two basins -separated by a shallow sill with no seismic penetration (Fig. 1D)- show a different seismic stratigraphy due to their complex bathymetry and variable sedimentological processes. The southern basin is characterized by the flat bottom areas in B1 and B2 (Fig. 1B and D), corresponding to the lutoclines (Canals et al., 1990), and extensive and rather flat areas at ~20 m water depth between and around these two main depressions, displaying moderate seismic penetration (Fig. 2). The bedrock surface was identified in a previous lower-frequency survey (150-2000 kHz) (Canals et al., 1990) and is characterized by local irregularities and discrete steps and sharp edges, consistent with the karstic origin and active dynamics of the two depressions.

Seismic stratigraphic analysis of our 3.5 kHz survey allowed the identification of three major seismic units (SA-SC; Figs. 2) and several seismic horizons, which have been tracked through the southern basin. These horizons and units were correlated with the core lithostratigraphy (see below). A constant acoustic velocity of 1500 m/sec based on the MSCL measurements has been used for the seismic-to-core correlation (Fig. 2A).

The oldest seismic unit (*Unit SA*) reaches more than 10 m thickness and is only recognizable in areas located close to the E lake margin. It is characterized by rather

continuous, mid-amplitude reflections and intercalated seismically more transparent units up to 2 m thick. The lowermost part of core BAN-11-1A reached the uppermost part of this seismic unit (Fig. 2A).

Unit SB is visible only in few areas and consists of continuous low-amplitude reflections with the intercalation of two higher amplitude reflections, coinciding with rather homogeneous lithology (Fig. 2A).

The youngest seismic unit (*Unit SC*) has been mapped through larger areas of the southern basin and reaches ~10 m in thickness in the central areas of the platforms. Seismic facies are characterized by the alternation of high-amplitude, laterally continuous reflections and transparent layers, slightly increasing basinward in thickness up to ~1 m thick (Fig. 2). The upper part of this seismic unit onlaps over SA and SB units and corresponds in sediment core 1A with a lithological change to sediments with higher and more variable density (Fig. 2A).

4.2 Sedimentology

4.2.1 Lithotypes

Six lithotypes have been defined in the long (BAN-11-1A) and short (BAN-12-1 to 8) sediment cores recovered from the southern areas of Lake Banyoles, on the basis of detailed sedimentological descriptions, smear-slide and SEM microscopic observations and compositional analyses. According to textural and compositional criteria, these lithotypes have been grouped into two main categories: i) banded to laminated and ii) massive (Table 1, Figs. 2, 3 and 4).

Banded and laminated lithotypes (Fig. 4A, B and C) are composed of variable amounts of: i) mud-size (10-15 μm) elongated Low Magnesium Calcite (LMC) crystals derived from direct precipitation from lake waters (Fig. 5B), ii) reworked biogenic particles

from the littoral areas (*Chara* fragments, micrite oncoids, ostracods and gastropod fragments of different sizes (<50 μm)); iii) diatoms and other organic components (Figs 5A, C.); and iv) detrital particles, including carbonates, quartz grains and clay minerals (mainly illite and chlorite) derived from the weathering and erosion of the soils and bedrock in the watershed (Figs. 3 and 5A). Grain-size distribution is dominated by the silt fraction, with mean values ranging from 5 (lithotype 1) to ~20 μm (lithotype 3) (Table 1, Fig. 3).

Massive lithotypes (Fig. 4D, E and F) occur as:

- i) up to 120 cm thick, fining upwards sequences, ranging from carbonate-rich sands (lithotypes 6, ~65 μm mean grain size) to fine-grained silts capped by clay-sized particles at the top (lithotype 5, ~10 μm mean grain size). These sediments are more carbonate-rich than banded and laminated lithotypes (Fig. 3) and contain higher amounts of coarse and fine-grained particles (from sands to silts) of reworked components (fragmented bioclasts, sub-rounded grains) (Fig. 5D, E and F). They are restricted to the lowermost part of the recovered succession and deposited by turbidity currents caused by the collapse of littoral areas (mass-wasting deposits) (Figs. 3 and 4F)
- ii) ‘homogenites’ (lithotype 4) occurring as 2 to ~75 cm-thick layers lacking any clear vertical grain-size distribution, composed of poorly sorted, fine-grained silts with mean sizes ranging from 6 to 12 μm (Figs. 3 and 4E). These layers are likely deposited after the fluidization of sediment particles maintained in suspension at the deepest sub-basins of the lake (B1 and B2) and they are more abundant in the upper part of the sequence. They are described in detail below.

4.2.2 Cores stratigraphy

According to their lithology (Table 1, Fig. 3), the sedimentary succession in the southern basin of Lake Banyoles has been divided into three main lithological units (LA, LB, LC) matching with facies associations.

Unit LA (1298 to 970 cm core depth,) is characterized by the presence of carbonate-rich, silty lithotype 3 at the base (Figs. 3 and 4C), leading to an alternation between more, fine-grained lithotype 1 and relatively thin beds of massive lithotype 4 at in the middle of this unit. A thick mass-wasting deposit (~120 cm), with a sandy layer at the base (lithotype 6) and massive lithotype 5 occurs in the uppermost part of this interval (Figs. 3 and 4F). This unit represents the transition from a relatively shallow, carbonate producing depositional environment with bioturbation and thus, oxic conditions (lithotype 3) to a relatively deeper setting (lithotype 1) accompanied by intensification of groundwater inflow (lithotype 4) and mass-wasting activity (lithotype 6).

Unit LB (972 to 610 cm core depth) is characterized by the deposition of carbonate-rich, silty lithotype 3 (Figs. 3 and 4C, Table 1), interbedding mm-thick layers of massive silts. This unit deposited in a shallow, carbonate producing, oxic depositional environments with abundant littoral fauna and variable detrital input.

Unit LC (610 to 0 cm core depth) starts with the deposition of banded to laminated lithotype 2, reflecting more oxygen-depleted conditions associated with more distal/offshore deeper depositional environments than Unit LB (Figs. 3 and 4B, Table 1). Upcore, sediments are composed by an alternation of cm-thick fine-grained sediments interval (lithotype 1) and thick layers of homogenites (lithotype 4) (Figs. 4D, E). This unit represents dominant distal deposition at the coring site away from the slope of the margin of the lake, with relatively low oxygenation conditions. The succession of lithotypes 3, 2 and 1 suggests a progressive increase in lake level, confirmed by the seismic onlapping of unit C onto B (Fig. 2). The deposition of up to 17 homogenite layers, with a maximum thickness of ~75 cm, also reflects

an abrupt intensification of groundwater activity during unit LC. The decrease in frequency and thickness of lithotype 4 layers in the uppermost part of the succession is interpreted as a decrease in groundwater activity in more recent times, accompanied by increased carbonate and organic content (Figs. 3 and 6A).

4. 3 Seismic to core correlation and depositional evolution

Seismic to core correlation enables a basin-wide reconstruction of the main stages in the Holocene depositional history of Lake Banyoles (**Fig. 2A**).

On the basis of seismic facies and the alternation of density contrasts, seismic Unit SA is interpreted as a sedimentary succession characterized by the intercalation of massive lithotypes (4, 5 and 6) within a sequence from distal-fine grained lithotype 1 to littoral carbonate-rich lithotype 3 (Figs. 2A and 3). Deposition of mass-wasting deposits and turbidites – as the one > 1 m thick turbidite (lithotypes 5 and 6) at the top of this unit - could have been more frequent during an early stage of development of the southern basin depressions with more active karstic collapses. Additionally, several relatively thin (up to 25 cm-thick) homogenites (lithotypes 4 and 5) also occur at the lowermost part of this unit (Fig. 2A and 3).

According to lithology, low-amplitude reflections with the intercalation of two higher amplitude reflections in SB are interpreted as the dominance of acoustically homogeneous, carbonate-rich lithotype 3 deposits with frequent clastic intercalations. A basinward increase in thickness (from ~4 m in coring location to more than 6 m in more distal areas) might be related to the occurrence of mass-wasting deposits at the lower part of the recovered sequence (Fig. 2).

Finally, seismic facies observed in uppermost unit SC correspond to the alternation between lithotype 1 and thick homogeneous lithotype 4 layers, characterized by higher and

constant density values (Fig. 2A). The onlapping of this unit above lowermost ones (A, B) suggest an increase of lake level associated with the deposition of more fine and distal lithotypes 1 and 4; higher groundwater flow (main water source of Lake Banyoles) is likely associated with these periods of higher lake level. Good lateral continuity of reflections and thickening of seismically transparent units towards the deepest sub-basin B2 suggests that the origin of homogeneous lithotype 4 is related to depositional processes around this sub-basin (Fig. 2).

4.4 Age model

To construct the age model, a total of 9 radiocarbon dates from core BAN-11-1A (Table 2) were used. Most of the dated samples correspond to bulk organic matter due to the absence of terrestrial organic macro remains. A large reservoir effect is suspected as recent sediments (44.5 cm depth) yielded an uncorrected age of 5460 ± 35 ^{14}C yr BP. To determine this reservoir effect and their likely variability through time, we used two dual dates, each of them from the same stratigraphic levels: i) at the top of the sequence, characterized by sedimentation under relatively deep conditions, similar to present-day (lithotypes 1 and 4), comparing ^{137}Cs maximum activity peak of 1963 AD and a radiocarbon date on bulk organic matter (reservoir effect = ~5470 yrs); and ii) at the base of the core, with predominantly shallow-water conditions (lithotypes 1, 2 and 4.2), comparing two radiocarbon dates derived from a terrestrial macro-remain and bulk organic matter (reservoir effect = ~3025 years) (Table 2).

The estimated reservoir effects for the top and the base of the core were subtracted from radiocarbon dates made on bulk organic matter at lithological units LC and LA-LB, respectively. A consistent result was obtained in lowermost units A and B, with a rather constant sedimentation rate of ~0.1 cm / year (Fig. 7A). The comparatively higher reservoir

effect obtained for the uppermost unit C, characterized by higher lake levels, might be explained by higher input of dissolved carbon from groundwater, likely higher during this recent stage. Variations in groundwater flow and potential reworking of organic particles from the deepest sub-basins B1 and B2 might also be responsible for the radiocarbon reversals occurring within unit A. Thus, the three radiocarbon dates of units A and B were considered for the chronology of the sequence, while all the other dates were rejected (Table 2, Fig. 7A).

Corrected dates were calibrated into calendar years and the age-depth relationship was constructed by linear interpolation (Fig. 7A). Event layers, deposited instantaneously and represented by massive lithotypes 4, 5 and 6 (i.e., homogenites in lithological units LA and LC (Fig. 7A, B) and the mass-wasting deposit at the top of unit A), were subtracted from the age model. According to this, the Lake Banyoles sequence spans the last ~7600 cal years BP. The uppermost unit LC was deposited during the last ~2800 cal years. The age-depth relationship shows an abrupt increase of sedimentation rate at the transition between units LB and LC, from 0.1 cm / year to 0.23 cm / year, including event layers (Fig. 7A). The abundance of these homogenites in the upper unit explains this sedimentary rate change (Fig. 7B). The internal chronology for the uppermost unit, between the uppermost validated date (~2800 cal yrs BP) and the 1963 AD maximum ^{137}Cs activity peak, remains unclear due to the lack of dates. Three different models can be used as an approximation: model 1) an extrapolation of ^{137}Cs inferred sedimentation rate throughout the interval containing the homogenites; model 2) an interpolation between ^{137}Cs peak and valid date (2800 cal yrs BP) at the uppermost part of unit B; and model 3) an interpolation between ^{137}Cs peak and lowermost (not valid) radiocarbon date of unit C. According to these different age models, the occurrence of homogenites could be restricted to the periods 1840-1938 AD, 380-1600 AD and 1340-1720 AD, respectively (Fig. 7B).

4.5 Sedimentological and geochemical characterization of homogenites

Lithotype 4 is dominant throughout the uppermost part of the sequence (lithological unit LC) (Figs. 3 and 6A) and is also present occasionally at the lowermost unit LA, recovered in the platform between deepest sub-basins B1 and B2. These intervals are defined by their regular colour, texture and composition, with minor or no internal variations. Compared to intercalated lithotype 1, they are characterized by a lighter colour (higher L* values, > 60), higher magnetic susceptibility (MS), higher density and a slightly coarser grain size, as evidenced by higher mode (~6 μm) and mean values (6 to 12 μm) (Figs. 3, 4E and 6A).

These homogenites are also characterized by a slightly higher organic and carbonate content (as recorded by TIC, calcite and higher Ca and Sr values) (Figs. 3 and 6A). Consequently, they have a relatively lower concentration on siliciclastic minerals (quartz and clay minerals) and elements associated with this fraction (Al, Si, K, Ti, Zr, Fe, Mn) as summarized by lower Ti/Ca values (Fig. 6B). Other geochemical properties characterizing lithotype 4 are: i) a lower Sr/Ca ratio, likely revealing a lower proportion of aragonite, common in biogenic particles mostly reworked from littoral, carbonate-producing areas of the lake; ii) higher S values; and iii) a higher Fe/Mn ratio, likely indicating more local anoxic conditions during the deposition of these layers (Fig. 6A).

Detailed inspection of SEM images supports previous textural and compositional analyses (Fig. 3) and reveal: i) slightly coarser grain size in homogenites than facies 1 (Figs. 5A, D), ii) more evidences of transport and reworking in homogenites (broken diatoms, irregularly shaped grains, etc.) (Figs. 5D, E, F), iii) a higher content of well-developed, endogenic and regular calcite crystals in lithotype 1 (Fig. 5B), iv) a higher content of pyrite framboids in homogenites likely related to higher S concentrations (Fig. 5E) and v) the exclusive presence of the most fragile terrestrial components (e.g., plant remains) in offshore/distal deposits of

lithotype 1 (Fig. 5C). Moreover, reworked planktonic calcareous algae remains exclusively occur in the homogenites of lithotype 4 (Fig. 5E).

Suspended sediments recovered below the lutoclines of the deepest sub-basins B1 and B2 show a very similar sedimentary features compared to homogenites, characterized by light grey colours (slightly reddish in B1 and bluish in B2) (Figs. 4G and H). Both homogenites and sediments from these sub-basins are, when compared with offshore/distal lithotype 1, characterized by higher carbonate content as reflected by higher Ca/Ti ratios (Fig. 6B). Average mean grain sizes in B1 and B2 average 8.6 and 9.6 μm , respectively, slightly coarser than in the homogenites (6.5 μm).

5. Discussion

5.1 Homogenites and fluidization events

Textural and compositional analyses of lithotype 4 deposits show a strong homogeneity along the whole layer, particularly visible within uppermost unit LC (Figs. 3 and 6A). Good lateral correlation of these ‘homogenites’ between long and short cores (Fig. 8) and inspection of seismic lines (Fig. 2) show that these deposits, absent in the northern basin of Lake Banyoles, appear clearly ‘thinning’ towards the edges of the southern basin and ‘ponding’ offshore towards deepest sub-basins B1 and B2 (Fig. 2 and 8). These layers are characterized by transparent seismic facies with no significant lateral changes (Fig. 2). The origin of homogenites is usually attributed to allochthonous (i.e., distal part of a turbidite initiated by a mass-wasting process in littoral areas turning into hyperpycnal (turbidity currents with bed-load and suspended load)) or autochthonous sources (liquefaction, resuspension) (Beck, 2009).

Turbidites are usually characterized by single, fining upwards sequences (Girardclos et al., 2007; Hsü and Kelts, 1985; Schnellmann et al., 2005). However, in Banyoles, only the

homogeneous layer located at the top of lithological unit LA displays these particular sedimentological features (Figs. 2A, 3 and 4F), and thus, is interpreted as a turbidite deposit likely triggered by a mass-wasting episode. On the other hand, considering the location of core BAN-11-1A, less than 100 m far from the lake shore, the presence of coarser grain particles at the base of these deposits would be also expected if the area source was the littoral of the lake, as described in other similar karstic lakes in the Iberian Peninsula (Morellón et al., 2009; Valero- Garcés et al., 2013).

In contrast to turbidite deposition, formation of homogenites in upper unit C involves liquefaction in the deeper sinkholes, resuspension of sediments and vertical transport and settling of the particles in the platform areas. In fact, these mechanisms of transport and deposition have been described for most of the deep sub-basins of the lake, with particular intensity for sub-basins B1 and B2 as a result of intense groundwater inflow (Serra et al., 2002; Soler et al., 2009). Fluidization and resuspension processes in lake sediments can also result from shaking caused by earthquakes. However, this process should be rejected since this region has a low to moderate seismic activity related to some Pyrenean Range faults and only few earthquakes have been described (Secanell et al., 2004). The only relatively intense ($M_w = 6.5$) earthquake recorded during historical times occurred in 1427 AD, with the epicenter located ~22 km SW to the lake (Olivera et al., 2006) and likely caused shaking in the lake basin. Nevertheless, given the low frequency of intense earthquakes and the high frequency of homogenite events, seismic activity in the area cannot be considered as the exclusive potential triggering mechanism for the deposition of this high number of homogenites.

Comparison of homogenites with sediments accumulated at the deepest sub-basins (B1 and B2), corresponding to cores BAN-12-1 and 2, reflects many textural and compositional similarities from the macroscopic scale, as observed in core images (Figs. 3, 4 and 6B) to the

microscopic level, as observed in SEM images. Although the range of variation in grain size is relatively small in general, and within unit C in particular, homogenites are slightly coarser (Fig. 3), with values closer to BAN-12-1 and 2, averaging 8.6 and 9.6 μm , respectively. From the compositional point of view, Ti/Ca ratios of lithotype 4 and short cores BAN-12-1 and 2 are also similar and generally lower than lithotype 1 (Fig. 6B). Thus, a common sediment source between B1 and B2 and homogenites is suggested. The marginal location of core BAN-11-1A within the flat platform between B1 and B2 might explain this decreasing grain size from B1 and B2 (8.6 μm and 9.6 μm), as coarsest particles transported by turbidity plumes do not probably reach this area, as predicted by previous studies (Serra et al., 2002; Serra et al., 2005).

According to recent limnological monitoring, there is a permanent contribution of sediment particles derived from turbidity plume developed above B1 (Colomer et al., 2001; Serra et al., 2005). Particle sediment fluxes in areas near coring site BAN-11-1A, close to the shallow platform margins, between B1 and B2, do not reach 5 $\text{g m}^{-2} \text{ day}^{-1}$ (Serra et al., 2002; Serra et al., 2005). Therefore, this plume might contribute to < 1 mm/year of sediment thickness in this area and thus, is responsible for a relatively low important contribution of particles, decreasing in size and number towards lake platform marginal areas, where coring site BAN-11-1A is located (Fig. 8). Consequently, the relatively low sedimentation rate produced by this plume is not able to accumulate the high thickness of homogenites sediment. In fact, reddish, massive grained silts derived from B1 are spatially restricted to the edges of this sub-basin and they do not normally reach more than 50 m far from the source area (Fig. 8). Furthermore, the frequent but episodic deposition of these homogenites must result from an episodic and relatively rapid process rather than from a continuous, variable permanent depositional mechanism.

In contrast, the second and stronger plume developed periodically above B2, as a result of extraordinary intense groundwater inflow caused by intense rainfall in the recharge area of the aquifer (Soler et al., 2009), has a particle sediment flux of $156 \text{ g m}^2 \text{ day}^{-1}$ (one order of magnitude higher than B1), so that it is able to accumulate more than 1 cm of sediments per year in the marginal areas of the platform located between B1 and B2. Taking into account that homogenite thicknesses display a high range of variability (from 2 to 76 cm) and the expected variability in the flow velocity for this turbidity plume, associated with the variable diameter of karstic conducts within B2, this is the most likely depositional mechanism able to produce homogenites.

In fact, correlation between short cores recovered between B1 and B2 and seismic line (Fig. 8) document how most of the uppermost homogenites (reflected as transparent seismic facies) are ponding predominantly towards sub-basin B2 and get thinner towards the edge of the lake and B1. This depositional pattern suggests fluidization and resuspension of sediments in sub-basin B2 as a result of particularly intense rainfall episodes in the recharge area of the aquifer as the most likely mechanism for the deposition of homogenites in Lake Banyoles.

5.2 Chronology and paleoenvironmental significance of homogenites

According to $^{137}\text{Cs}/^{210}\text{Pb}$ dating, no discrete layers associated with the 11 fluidization events monitored in B2 during the period 1976-2004 AD (Soler et al., 2007) have been recorded in core BAN-11-1A (Fig. 7). However, a detailed inspection of core images reveals an internal irregular ‘sublayering’ of mm to sub-mm thick laterally uncontinuous light grey silts within black, massive, carbonate-rich silts of lithotype 1 (Fig. 4A and 8B). These small amounts of light grey silt sediments might be derived from sub-basin B2 and have reached coring site. Therefore, more intense groundwater inflow (or smaller karstic subaqueous springs within sub-basin B2) is required to produce a denser turbidity plume than the ones

monitored during the last years (Soler et al., 2007) so that these 17 layers within uppermost unit LC could be deposited. Alternatively, a longer duration for these events could produce thick homogenite layers. However, we would expect some internal structure in the sediment layers if the events lasted several years, and the lack of clear internal structure within these layers make such a long lasting, permanent turbidity plume rather unlikely.

The different age models proposed for the uppermost unit containing the homogenites (Fig. 7B), indicate that they were deposited between the 4th and 20th centuries AD. Chronological uncertainties associated with the lack of reliable radiocarbon dates within this interval hamper an accurate dating of these depositional events. In model 1, $^{137}\text{Cs} - ^{210}\text{Pb}$ inferred sedimentation rate is unlikely to remain constant throughout several millennia characterized by changing land use and climate. According to model 2, the linear interpolation with the validated date of ~2800 cal yrs BP implies an unlikely abrupt change prior to 1963 AD and also a constant sedimentation rate through the intervals containing different lithologies: i) alternating lithotypes 1 and 4 (upper part of the succession) and ii) banded to laminated lithotype 2 (lower part of the succession). Finally, the exclusive validation of the lowermost radiocarbon date within unit LC is arbitrary as all the others were rejected for the potential recycling of material derived from resuspension (Table 2, Fig 7).

A fluctuating, long-term increase in lake level in Banyoles is evidenced by the onlapping of unit LC over units LA and LB, containing shallower deposits (Figs. 2 and 3). This is also supported by the existence of a submerged Neolithic settlement in the eastern shore of the lake (La Draga site). This archeological site is constituted by lakeshore type houses dated as old as ~7200 cal. BP (Bosch et al., 2000; Tarrús, 2008), and implies that lake level was up to 1.5 m lower than the current level during the Neolithic .

A drastic change in depositional environments occurred at the base of Unit C, at ~2.8 cal ka BP, and inaugurated a new lake dynamics favorable to homogenite formation. Although

the timing is coherent with a large increase in humidity - particularly in southern Spain (Martín-Puertas et al., 2009) –documented at the onset of the Iberian-Roman Humid Period (ca. 2.5 cal ka BP), moisture conditions have been quite variable during the last 2 millennia in the Iberian Peninsula in general (Moreno et al., 2012) and NE Spain in particular (Morellón et al., 2012). Thus, a direct, exclusive climate driven hydrological change for the deposition of homogenites can be ruled out. However we cannot discard the possibility that changes in the karst functioning with new preferential areas for spring flow brought by the onset of this humid period could have become permanent and favored homogenite formation during the last 3 millennia.

The presence of several homogenites at the lowermost part of the recovered sequence, between ~5450 and 7200 cal yrs BP suggest that, apart from the autogenic evolution of these karstic depressions described by Canals et al. (1990), an external hydrological mechanism would be required for such a depositional change. In fact, no homogenites have been identified near to the other sub-basins of the lake by geophysical surveys and sediment cores. Thus, a higher, local groundwater discharge likely caused by a faster recharge of the aquifer might have activated sub-basin B2, causing these episodic, more intense fluidization events and associated turbidity plumes in Lake Banyoles during the last millennia. Without a more detailed age model, the onset of homogenite deposition could have started as early as the humid Iberian-Roman Period or as late as Medieval times. In the second case, it would have been coincident with the human settlement of the area and associated changes in land use and lake hydrology. The foundation of Sant Esteve Monastery in the town of Banyoles (Sanz i Alguacil, 1991) in the early 9th century AD lead to large changes in the lake and the watershed, as the construction of an artificial drainage system (five artificial outlets and several dikes in the eastern shore of the lake) to control lake level. Moreover, intense deforestation and farming affected the catchment drainage and permeability. A local

expansion of agriculture occurred in relation to the foundation of another Romanesque monastery in the town of Besalu (960 AD), located in the recharge area of the aquifer (Sanz, 1981).

Deforestation caused by the important expansion of farmlands in the region and associated increase in soil permeability in the recharge area of the aquifer might have led to a faster recharge of the karstic system feeding Lake Banyoles, increasing its rapid hydrological response to intense rainfall episodes responsible for fluidization episodes in sub-basin B2 and favoring the deposition of homogenites. Higher groundwater inflow through the spring located in sub-basin B2 could be responsible for more intense fluidization events and associated turbidity plumes. Progressive farmland abandonment and associated reforestation during the mid to late 20th century and/or groundwater extraction might have lowered water table, decreasing the intensity of fluidization events in B2 sub-basin during recent times and thus, preventing the deposition of homogenites.

6. Conclusions

Recent sedimentary processes in karstic Lake Banyoles are strongly influenced by the effect of groundwater activity, which leads to fluidization, re-suspension and mainly vertical transport and gravity of sediment particles forming homogenite deposits accumulated in the platforms between deepest sub-basins B1 and B2. These processes are permanent in B1 and periodical in B2, respectively. Based on high-resolution geophysical surveys and detailed sedimentological and geochemical analyses of several cores, we document a large variability in the intensity and frequency of these transport processes and the subsequent deposition of homogenite layers during the last millennia.

The ~7.6 cal kyr BP recovered sequence of Lake Banyoles has recorded an increase in lake level after ~2800 cal yrs BP, as indicated by geophysical (i.e., the onlapping of

uppermost unit SC onto lowermost units SA and SB) and sedimentological (i.e., change from massive, carbonate-rich shallow lake deposits into fine-grained, clastic-rich sediments) evidences. This lake level change was accompanied by a subsequent intensification of groundwater input and the deposition of up to 75 cm thick 17 layers of homogenites.

Textural and compositional analysis and depositional patterns of homogenites indicate that they have been deposited by periodical, intense, fluidization events in sub-basin B2 as those described and monitored for recent times. Intensity, however, was higher, able to generate thicker, discrete layers in marginal areas of the platform between the deepest sub-basins in the southern basin of the lake. The onset of these events was triggered by higher and more intense local, groundwater inflow and might be related to agricultural expansion during Roman and/or medieval times in the region. Increased farmland surface in the recharge area of the aquifer increased soil permeability and subsequently, the rapid response of the aquifer to intense rainfall episodes in the recharge area.

Acknowledgements

Financial support for research was provided by the Spanish Inter-Ministry Commission of Science and Technology (CICYT), through the projects GLOBALKARST (CGL2009-08415) and GRACCIE-CONSOLIDER (CSD2007-00067). Additional funding was provided by INTIMATE-COST through a travel grant ‘Short Term Scientific Mission, COST Action ES0907’ in 2011 at IPE-CSIC and University of Barcelona (Spain).

M. Morellón and F. Barreiro hold ‘JAE-DOC’ and ‘JAE-PREDOC’ pre and postdoctoral contracts, respectively, both co-funded by C.S.I.C. and the European Social Fund. We acknowledge the Town Hall of Banyoles (Girona) and Club Natació Banyoles for their collaboration in fieldwork activities and Jaime Frigola and Pol Tarrats (Univ. of Barcelona), and Miguel Sevilla and Josu Aranbarri (IPE-CSIC) for coring assistance in 2011.

We are also grateful to Irene Brunner, Silvia Bollhalder, Marian Fujak, Alois Zwyssig and Brian Sinnet (Eawag, Switzerland); Adrian Gilli and Stephanie Wirth (ETH-Zürich, Switzerland) and Beatriz Bueno, Aida Adsuar and Miguel Bartolomé (IPE-CSIC, Spain) for their laboratory assistance and collaboration in this research. We thank constructive comments on the manuscript made by Maria Rieradevall (Univ. of Barcelona).

REFERENCES

- Álvarez-Cobelas, M., Rojo, C., Angeler, D.G., 2005. Mediterranean limnology: current status, gaps and the future. *Journal of Limnology*, 64(1): 13-29.
- Assayag, N., Jézéquel, D., Ader, M., Viollier, E., Michard, G., Prévot, F., Agrinier, P., 2008. Hydrological budget, carbon sources and biogeochemical processes in Lac Pavin (France): Constraints from $\delta^{18}\text{O}$ of water and $\delta^{13}\text{C}$ of dissolved inorganic carbon. *Applied Geochemistry*, 23(10): 2800-2816.
- Barnolas, A., 1992. Evolución sedimentaria de la Cuenca Surpirenaica Oriental durante el Eoceno. *Acta Geologica Hispanica*, 27(1-2): 15-31.
- Beck, C., 2009. "Late Quaternary lacustrine paleo-seismic archives in north-western Alps: Examples of earthquake-origin assessment of sedimentary disturbances". *Earth-Science Reviews*, 96(4): 327-344.
- Bischoff, J.L., Julià, R., Shanks, W.C., Rosenbauer, R.J., 1994. Karstification without carbonic acid: Bedrock dissolution by gypsum-driven dedolomitization. *Geology*, 22(11): 995-998.
- Bloesch, J., 1995. Mechanisms, measurement and importance of sediment resuspension in lakes. *Marine and Freshwater Research*, 46(1): 295-304.

- 722 Bosch, A., Chinchilla, J., Tarrús, J., 2000. El Poblado Lacustre Neolític de la Draga:
723 Excavacions de 1990 a 1998. Museu d'Arqueologia de Catalunya-Centre
724 d'Arqueologia Subaquàtica de Catalunya, Girona, Girona (Spain).
- 725 Brusi, D., Bach, J., Sanz, M., 1990. Itinerari geològic de Banyoles. Descoberta del
726 funcionament del sistema lacustre. Apunts 22. Eumo Editorial, Barcelona, 124 pp.
- 727 Burbank, D.W., Puigdefàbregas, C., Muñoz, J.A., 1992. The chronology of the Eocene
728 tectonic and stratigraphic development of the eastern Pyrenean foreland basin,
729 northeast Spain. Geological Society of America Bulletin, 104(9): 1101-1120.
- 730 Burne, R.V., Moore, L.S., 1987. Microbialites; organosedimentary deposits of benthic
731 microbial communities. PALAIOS, 2(3): 241-254.
- 732 Canals, M., Got, H., Julia, R., Serra, J., 1990. Solution-collapse depressions and suspensates
733 in the limnogenic lake of Banyoles (NE Spain). Earth Surface Processes and
734 Landforms, 15(3): 243-254.
- 735 Casamitjana, X., Colomer, J., Roget, E., Serra, T., 2006. Physical Limnology in Lake
736 Banyoles. Limnetica, 25(1-2): 181-188.
- 737 Casamitjana, X., Colomer, J., Roget, E., Teresa, S., 1996. On the presence of aggregates in
738 the basins of Lake Banyoles. Geophysical Research Letters, 23(20): 2737-2740.
- 739 Casamitjana, X., Roget, E., 1993. Resuspension of sediment by focused groundwater in Lake
740 Banyoles. Limnology and Oceanography, 38(3): 643-656.
- 741 Colomer, J., Ross, J.A., Casamitjana, X., 1998. Sediment entrainment in karst basins. Aquatic
742 Sciences, 60(4): 338-358.
- 743 Colomer, J., Serra, T., Piera, J., Roget, E., Casamitjana, X., 2001. Observations of a
744 hydrothermal plume in a karstic lake. Limnology and Oceanography, 46(1): 197-203.
- 745 Colomer, J., Serra, T., Soler, M., Casamitjana, X., 2002. Sediment fluidization events in a
746 lake caused by large monthly rainfalls. Geophys. Res. Lett., 29(8): 1260.

- 747 Coma, M.V., Abella, C.A., Oromi, O., 1988. Caracteritzacio fisico-quimica dels travertins en
748 formació de l'Estany de Banyoles. *Scientia gerundensis*, 14: 43-56.
- 749 Coma, M.V., Oromi, O., Abella, C.A., 1987. Cartografia dels travertins en formació de
750 l'Estany de Banyoles. *Scientia gerundensis*, 13: 65-74.
- 751 Cho Martínez, S., 2012. Registros sedimentarios como indicadores paleoambientales y de
752 actividad antrópica en el Neolítico del Lago de Banyoles. Master Thesis, Universidad
753 de Burgos Burgos (Spain), 48 pp.
- 754 Chung, F.H., 1974a. Quantitative interpretation of X-ray diffraction patterns of mixtures. I.
755 Matrix-flushing method for quantitative multicomponent analysis. *Journal of Applied*
756 *Crystallography*, 7(519-525).
- 757 Chung, F.H., 1974b. Quantitative interpretation of X-ray diffraction patterns of mixtures. II.
758 Adiabatic principle of X-ray diffraction analysis of mixtures. *Journal of Applied*
759 *Crystallography*, 7: 526-531.
- 760 Dadheech, P.K., Glöckner, G., Casper, P., Kotut, K., Mazzoni, C.J., Mbedi, S., Krienitz, L.,
761 2013. Cyanobacterial diversity in the hot spring, pelagic and benthic habitats of a
762 tropical soda lake. *FEMS Microbiology Ecology*, 85(2): 389-401.
- 763 Descy, J.-P., Darchambeau, F., Schmid, M., 2012a. Lake Kivu Research: Conclusions and
764 Perspectives. In: J.-P. Descy, F. Darchambeau, M. Schmid (Eds.), *Lake Kivu. Aquatic*
765 *Ecology Series*. Springer Netherlands, pp. 181-190.
- 766 Descy, J.-P., Darchambeau, F., Schmid, M. (Eds.), 2012b. *Lake Kivu. Limnology and*
767 *biogeochemistry of a tropical great lake. Aquatic Ecology Series*, 5. Springer.
- 768 Draganits, E., Janda, C., 2003. Subaqueous artesian springs and associated spring pits in a
769 Himalayan pond. *Boreas*, 32(2): 436-442.
- 770 Dutras, A., Abella, C., Brunet, R., 1986. Determinació del sistema de corrents a l'Estany de
771 Banyoles en condiciones de calma meteorològica estival. In: D.d. Girona (Ed.),

- 772 Primeres jornades sobre l'Estany de Banyoles. Ponències i comunicacions, Banyoles
773 (Spain), pp. 149-157.
- 774 Edmunds, W.M., Dodo, A., Djoret, D., Gaye, C., Goni, I., Travi, Y., Zouari, K., Zuppi, G.-
775 M., Gasse, F., 2004. Groundwater as an archive of climatic and environmental change:
776 Europe to Africa. In: R. Battarbee, F. Gasse, C. Stickley (Eds.), Past Climate
777 Variability through Europe and Africa. Developments in Paleoenvironmental
778 Research. Springer Netherlands, pp. 279-306.
- 779 Garcia-Gil, L.J., Borrego, C.M., Bañeras, L., Abella, C.A., 1993. Dynamics of Phototrophic
780 Microbial Populations in the Chemocline of a Meromictic Basin of Lake Banyoles.
781 Internationale Revue der gesamten Hydrobiologie und Hydrographie, 78(2): 283-294.
- 782 García-Ruiz, J.M., López-Moreno, J.I., Vicente-Serrano, S.M., Lasanta-Martínez, T.,
783 Beguería, S., 2011. Mediterranean water resources in a global change scenario. Earth-
784 Science Reviews, 105(3-4): 121-139.
- 785 Girardclos, S., Schmidt, O.T., Sturm, M., Ariztegui, D., Pugin, A., Anselmetti, F.S., 2007.
786 The 1996 AD delta collapse and large turbidite in Lake Brienz. Marine Geology,
787 241(1-4): 137-154.
- 788 Guerrero, R., Abella, C., Miracle, M.R., 1978. Spatial and temporal distribution of bacteria in
789 a meromictic karstic lake basin: relationships with physicochemical parameters and
790 zooplankton. Verhandlungen des Internationalen Verein Limnologie, 20(2264-2271).
- 791 Höbig, N., Weber, M.E., Kehl, M., Weniger, G.-C., Julià, R., Melles, M., Fülöp, R.-H.,
792 Vogel, H., Reicherter, K., 2012. Lake Banyoles (northeastern Spain): A Last Glacial to
793 Holocene multi-proxy study with regard to environmental variability and human
794 occupation. Quaternary International, 274(0): 205-218.
- 795 Hsü, K.J., Kelts, K., 1985. Swiss lakes as a geological laboratory. Naturwissenschaften, 72(6):
796 315-321.

- 797 Ionescu, D., Siebert, C., Polerecky, L., Munwes, Y.Y., Lott, C., Häusler, S., Bižić-Ionescu,
798 M., Quast, C., Peplies, J., Glöckner, F.O., Ramette, A., Rödiger, T., Dittmar, T., Oren,
799 A., Geyer, S., Stärk, H.-J., Sauter, M., Licha, T., Laronne, J.B., de Beer, D., 2012.
800 Microbial and Chemical Characterization of Underwater Fresh Water Springs in the
801 Dead Sea. PLoS ONE, 7(6): e38319.
- 802 Julià-Brugués, R., 1977. Nuevos datos sobre la posición cronoestratigráfica de los materiales
803 cuaternarios de la cuenca lacustre de Banyoles-Besalú (Girona). Acta Geológica
804 Hispánica XII(1-3): 55-59.
- 805 Julia Brugués, R., Suc, J.-P., 1980. Analyse pollinique des dépôts lacustres du Pléistocène
806 inférieur de Banyoles (Bañolas, site de la Bòbila Ordis - Espagne): un élément
807 nouveau dans la reconstitution de l'histoire paléoclimatique des régions
808 méditerranéennes d'Europe occidentale. Geobios, 13(1): 5-19.
- 809 Julià, R., 1980. La conca lacustre de Banyoles Centro d'Estudios Comarcals de Banyoles,
810 Besalú, 188 pp.
- 811 Julià, R., Bischoff, J.L., 1991. Radiometric dating of quaternary deposits and the hominid
812 mandible of lake banyolas, Spain. Journal of Archaeological Science, 18(6): 707-722.
- 813 Leroy, S.A.G., 1997. Climatic and non-climatic lake-level changes inferred from a Plio-
814 Pleistocene lacustrine complex of Catalonia (Spain): palynology of the Tres Pins
815 sequences. Journal of Paleolimnology, 17(4): 347-367.
- 816 Løvlie, R., Leroy, S., 1995. Magnetostratigraphy of Lower Pleistocene Banyoles palaeolake
817 carbonate sediments from Catalonia, NE Spain: Evidence for relocation of the Cobb
818 Mountain sub-chron. Quaternary Science Reviews, 14(5): 473-485.
- 819 MAGRAMA, 2006. Information Sheet on Ramsar Wetlands: Lake Banyoles, pp. 21.
- 820 Martín-Puertas, C., Valero-Garcés, B.L., Brauer, A., Mata, M.P., Delgado-Huertas, A.,
821 Dulski, P., 2009. The Iberian-Roman Humid Period (2600-1600 cal yr BP) in the

- 822 Zoñar Lake varve record (Andalucía, southern Spain). *Quaternary Research*, 71(2):
823 108-120.
- 824 Mató i Palós, E., Saula i Briansó, E., Picart i Boira, J., Solà i Subiranas, J., Montaner i
825 Roviras, J., Viñals i Gisbert, E., Samsó i Escolá, J.M., Serra i Kiel, J., Llenas i
826 Abellaneda, M., Agustí i Ballester, J., Mallarach i Carrera, J., 1996. Banyoles 295-2-1
827 (76,23). In: X. Berástegui Batalla, M. Losantos Sistach, J. Cirés (Eds.), *Mapa geològic*
828 *de Catalunya 1:25000*. Generalitat de Catalunya, Departament de Política Territorial i
829 Obres Públiques, Institut Cartogràfic de Catalunya, Servei Geològic de Catalunya,
830 Barcelona (Spain).
- 831 Matter, M., Anselmetti, F.S., Jordanoska, B., Wagner, B., Wessels, M., Wüest, A., 2010.
832 Carbonate sedimentation and effects of eutrophication observed at the Kališta
833 subaquatic springs in Lake Ohrid (Macedonia). *Biogeosciences*, 7(11): 3755-3767.
- 834 Morellón, M., Pérez-Sanz, A., Corella, J.P., Büntgen, U., Catalán, J., González-Sampériz, P.,
835 González-Trueba, J.J., López-Sáez, J.A., Moreno, A., Pla-Rabes, S., Saz-Sánchez,
836 M.Á., Scussolini, P., Serrano, E., Steinhilber, F., Stefanova, V., Vegas-Vilarrúbia, T.,
837 Valero-Garcés, B., 2012. A multi-proxy perspective on millennium-long climate
838 variability in the Southern Pyrenees. *Clim. Past*, 8(2): 683-700.
- 839 Morellón, M., Valero-Garcés, B., Anselmetti, F., Ariztegui, D., Schnellmann, M., Moreno, A.,
840 Mata, P., Rico, M., Corella, J.P., 2009. Late Quaternary deposition and facies model
841 for karstic Lake Estanya (North-eastern Spain). *Sedimentology*, 56(5): 1505-1534.
- 842 Moreno-Amich, R., García-Berthou, E., 1989. A new bathymetric map based on echo-
843 sounding and morphometrical characterization of the Lake of Banyoles (NE-Spain).
844 *Hydrobiologia*, 185: 83-90.
- 845 Moreno, A., Pérez, A., Frigola, J., Nieto-Moreno, V., Rodrigo-Gámiz, M., Martrat, B.,
846 González-Sampériz, P., Morellón, M., Martín-Puertas, C., Corella, J.P., Belmonte, Á.,

- 847 Sancho, C., Cacho, I., Herrera, G., Canals, M., Grimalt, J.O., Jiménez-Espejo, F.,
 848 Martínez-Ruiz, F., Vegas-Vilarrúbia, T., Valero-Garcés, B.L., 2012. The Medieval
 849 Climate Anomaly in the Iberian Peninsula reconstructed from marine and lake records.
 850 Quaternary Science Reviews, 43(0): 16-32.
- 851 Olivera, C., Redondo, E., Lambert, J., Riera, A., Roca, A., 2006. Els terratrèmols dels segles
 852 XIV i XV a Catalunya. Institut Cartogràfic de Catalunya, Barcelona.
- 853 Paillard, D., Labeyrie, L., Yiou, P., 1996. Analyseries 1.0: a Macintosh software for the
 854 analysis of geographical time-series. Eos, 77: 379.
- 855 Pérez-Obiol, R., Julià, R., 1994. Climatic Change on the Iberian Peninsula Recorded in a
 856 30,000-Yr Pollen Record from Lake Banyoles. Quaternary Research, 41(1): 91-98.
- 857 Prat, N., Rieradevall, M., 1995. Life cycle and production of Chironomidae (Diptera) from
 858 Lake Banyoles (NE Spain). Freshwater Biology, 33(3): 511-524.
- 859 Reimer, P.J., Baillie, M.G.L., Bard, E., Bayliss, A., Beck, J.W., Blackwell, P.G., Ramsey,
 860 C.B., Buck, C.E., Burr, G.S., Edwards, R.L., Friedrich, M., Grootes, P.M., Guilderson,
 861 T.P., Hajdas, I., Heaton, T.J., Hogg, A.G., Hughen, K.A., Kaiser, K.F., Kromer, B.,
 862 McCormac, F.G., Manning, S.W., Reimer, R.W., Richards, D.A., Southon, J.R.,
 863 Talamo, S., Turney, C.S.M., van der Plicht, J., Weyhenmeyer, C.E., 2009. IntCal09
 864 and Marine09 Radiocarbon Age Calibration Curves, 0-50,000 Years cal BP.
 865 Radiocarbon, 51(4): 1111–1150.
- 866 Rieradevall, M., Roca, J.R., 1995. Distribution and population dynamics of ostracodes in a
 867 Karstic lake: Lake Banyoles (Catalonia, Spain). Hidrobiología, 310(3): 189-196.
- 868 Roget, E., Colomer, J., Casamitjana, X., Llebot, J.E., 1993. Bottom currents induced by
 869 baroclinic forcing in Lake Banyoles (Spain). Aquatic Sciences - Research Across
 870 Boundaries, 55(3): 206-227.

- 871 Rosen, M.R., Arehart, G.B., Lico, M.S., 2004. Exceptionally fast growth rate of <100-yr-old
872 tufa, Big Soda Lake, Nevada: Implications for using tufa as a paleoclimate proxy.
873 *Geology*, 32(5): 409-412.
- 874 Rosen, M.R., Chagué-Goff, C., Eser, P., Coshell, L., 2002. Utilisation of the sedimentological
875 and hydrochemical dynamics of the Stump Bay Wetland along Lake Taupo, New
876 Zealand, for the recognition of paleo-shoreline indicators. *Sedimentary Geology*,
877 148(1–2): 357-371.
- 878 Ross, K.A., Smets, B., De Batist, M., Schmid, M., Anselmetti, F.S., in review.
879 Morphobathymetry of Lake Kivu and its implications for lake-level history,
880 subaquatic volcanism and natural hazard assessment. *Earth and Planetary Science*
881 *Letters*.
- 882 Sanz i Alguacil, A., 1991. *Catalunya Romanica*. Vol V. El Gironès, la Selva, el Pla de
883 l'Estany, Enciclopèdia Catalana.
- 884 Sanz, M., 1981. El sistema hidrogeològic de Banyoles-La Garrotxa. Unpublished PhD thesis,
885 Universitat Autònoma de Barcelona, Barcelona, Spain.
- 886 Saula, E., Picart, J., Mato, E., Llenas, M., Lozanitos, M., Beràstegui, X., Agustí, J., 1994.
887 Evolución geodinámica de la fosa del Empordà y las Sierras Transversales. *Acta*
888 *Geologica Hispanica*, 29(2-4): 55-75.
- 889 Schnellmann, M., Anselmetti, F.S., Giardini, D., McKenzie, J.A., 2005. Mass movement-
890 induced fold-and-thrust belt structures in unconsolidated sediments in Lake Lucerne
891 (Switzerland). *Sedimentology*, 52(2): 271-289.
- 892 Schnurrenberger, D., Russell, J., Kelts, K., 2003. Classification of lacustrine sediments based
893 on sedimentary components. *Journal of Paleolimnology*, 29: 141-154.

- 894 Secanell, R., Goula, X., Susagna, T., Fleta, J., Roca, A., 2004. Seismic hazard zonation of
895 Catalonia, Spain, integrating random uncertainties. *Journal of Seismology*, 8(1): 25-
896 40.
- 897 Serra-Kiel, J., Travé, A., Mató, E., Saula, E., Ferràndez-Cañadell, C., Busquets, P., Tosquella,
898 J., Vergés, J., 2003. Marine and Transitional Middle/Upper Eocene Units of the
899 Southeastern Pyrenean Foreland Basin (NE Spain). *Geologica Acta*, 1(2): 177-200.
- 900 Serra, T., Colomer, J., Gacia, E., Soler, M., Casamitjana, X., 2002. Effects of a turbid
901 hydrothermal plume on the sedimentation rates in a karstic lake. *Geophys. Res. Lett.*,
902 29(21): 2029.
- 903 Serra, T., Soler, M., Julià, R., Casamitjana, X., Colomer, J., 2005. Behaviour and dynamics of
904 a hydrothermal plume in Lake Banyoles, Catalonia, NE Spain. *Sedimentology*, 52(4):
905 795-808.
- 906 Shapley, M.D., Ito, E., Donovan, J.J., 2005. Authigenic calcium carbonate flux in
907 groundwater-controlled lakes: Implications for lacustrine paleoclimate records.
908 *Geochimica et Cosmochimica Acta*, 69(10): 2517-2533.
- 909 Soler, M., Serra, T., Casamitjana, X., Colomer, J., 2009. High sedimentation rates in a karstic
910 lake associated with hydrothermal turbid plumes (Lake Banyoles, Catalonia, NE
911 Spain). *Sedimentary Geology*, 222(1-2): 5-15.
- 912 Soler, M., Serra, T., Colomer, J., Romero, R., 2007. Anomalous rainfall and associated
913 atmospheric circulation in the northeast Spanish Mediterranean area and its
914 relationship to sediment fluidization events in a lake. *Water Resour. Res.*, 43(1):
915 W01404.
- 916 Tarrús, J., 2008. La Draga (Banyoles, Catalonia), an Early Neolithic Lakeside Village in
917 Mediterranean Europe. *Catalan historical review*, 1: 17-33.

- 918 Tassone, A., Roca, E., Muñoz, J.A., Cabrera, L., Canals, M., 1994. Evolución del sector
919 septentrional del margen continental catalán durante el Cenozoico *Acta Geologica*
920 *Hispanica*, 29(2-4): 3-7.
- 921 Valero- Garcés, B., Morellón, M., Moreno, A., Corella, P., Martín-Puertas, C., Barreiro, F.,
922 Pérez, A., Giralt, S., Mata-Campo, M.P., 2013. The carbonate factory in karst lakes:
923 sources, processes and depositional environments in Quaternary Iberian Lakes.
924 *Sedimentary Geology*, in press.
- 925 Valero-Garcés, B., Zeroual, E., Kelts, K., 1998. Arid phases in the Western Mediterranean
926 Region during the last glacial cycle reconstructed from lacustrine records. In: G.
927 Benito, Baker, V.R., Gregory, K.J. (Ed.), *Palaeohydrology and Environmental*
928 *Change*. John Wiley & Sons Ltd., pp. 67-80.
- 929 Warren, J.K., 1982. The hydrological significance of Holocene tepees, stromatolites, and
930 boxwork limestones in coastal salinas in South Australia. *Journal of Sedimentary*
931 *Research*, 52(4): 1171-1201.
- 932 Winter, T.C., 1999. Relation of streams, lakes, and wetlands to groundwater flow systems.
933 *Hydrogeology Journal*, 7(1): 28-45.
- 934 Younger, P.L., Teutsch, G., Custodio, E., Elliot, T., Manzano, M., Sauter, M., 2002.
935 Assessments of the sensitivity to climate change of flow and natural water quality in
936 four major carbonate aquifers of Europe. Geological Society, London, *Special*
937 *Publications*, 193(1): 303-323.
- 938
- 939

TABLE CAPTIONS

<i>Lithotype</i>	<i>Sedimentological features</i>	<i>Compositional parameters</i>	<i>Depositional subenvironment/ process</i>
<i>Banded and laminated</i>	1 <i>Dark-grey to black, massive to banded, carbonate-rich silts with diatoms</i> Fine grained carbonate mud composed by up to 10 µm hexagonal calcite grains with abundant to frequent ca. 50-60 µm reworked occasional reworked littoral carbonate-rich particles (ostracods, charophytes and carbonate coatings). Frequent ca. 25 µm detrital carbonate particles, plant remains and diatoms, locally abundant. Occasional quartz grains and < 20µm pyrite framboids.	TIC = 3.3% - 6.7 % TOC = 0.0% - 1.2 % Mean GS = 5 – 18 µm Mineralogy: Cc= 42.3%, Ill = 32.5%, Chl = 17.7%, Qtz = 7.4%	Deep, monomictic, occasionally anoxic brackish to freshwater lake with permanent, low-concentration turbidity plumes
	2 <i>Laminated fcs comprising alternating mm to 1 cm thick black and light-grey fine-grained silts</i> Black laminae: Fine-grained (up to 10 µm) hexagonal to sub-hexagonal calcite grains with abundant diatoms, up to 100 µm reworked littoral carbonate particles and frequent 20-30 µm detrital grains of quartz and carbonates. Light grey laminae: fine-grained, up to 10 µm irregular, reworked calcite crystals with frequent up to 40 µm clastic quartz and non-biogenic carbonates. Occasional to frequent up to 50 µm reworked littoral carbonate-rich particles.	TIC = 3.9 % – 6.2 % TOC = 0.2 %- 1.1 % Mean GS = 6.0 – 8.4 µm Mineralogy: Cc = 39.5%, Ill = 32.7%, Chl = 19.5%, Qtz = 8.2%	Relatively deep, carbonate-producing lake with seasonal anoxic hypolimnetic conditions
	3 <i>Grey, barely laminated to massive, carbonate-rich silts with evidences of bioturbation</i> 30-50 µm reworked biogenic carbonate particles with abundant up to 50 µm irregularly shaped detrital grains of quartz and carbonates. Frequent fine-grained, up to 10 µm calcitic mud.	TIC = 4.4% – 9.3% TOC = 0.3%- 1.0 % Mean GS =4.8 – 18.9 µm Mineralogy: Cc = 51.6%, Ill = 26.5%, Chl = 15.1%, Qtz = 6.9%	Shallow, carbonate-producing brackish lake with oxic conditions
<i>Massive</i>	4 <i>Light grey, massive fine-grained, carbonate-rich silts, occurring as mm to cm-thick intercalations or cm to dm-thick homogeneous layers</i> Up to 10 µm fine-grained irregularly-shaped calcite mud with abundant reworked diatoms. Frequent up to 50 µm reworked carbonate particles, sub-circular calcareous algae and pyrite framboids. Occasional plant remains.	TIC = 4.3% -6.8 % TOC = 0.1% - 0.9 % Mean GS = 5 – 12.6 µm Mineralogy: Cc = 44.7%, Ill = 31.7%, Chl = 16.2%, Qtz = 7.4%	Fluidization events and associated periodical and intense turbidity plumes

5	<i>Light grey/yellowish, massive, fine-grained, up to 1 m thick fining upwards sequences ranging from coarse to fine-grained silts</i> Dominant 10-15 µm reworked, sub-rounded to hexagonal calcite grains with reworked littoral carbonate-rich particles (up to 50-60 µm), more frequent towards the base.	TIC = 4.5 % - 7.3% TOC = 0.3 % - 0.6 % Mean GS = 8.2 – 13.0 µm Mineralogy: Cc = 40.9%, Ill = 32.7%, Chl = 18.8%, Qtz = 7.7%	Mass-wasting processes
6	<i>Light grey/yellowish, massive, fine-grained, carbonate-rich sands</i> 100-300 µm sub-rounded, biogenic, reworked carbonate particles with abundant up to 100 µm coarse, high relief detrital grains of quartz and non-biogenic carbonates. Abundant fine-grained matrix composed of up to 10 µm sub-rounded calcite crystals.	TIC = 7.2% - 8.8% TOC = 0.4% - 0.5 % Mean GS = 65.5 µm Mineralogy: Cc = 57.9%, Chl = 18.1%, Ill = 15.4%, Qtz = 8.6%	Mass-wasting processes

Table 1. Lithotypes defined for the Lake Banyoles sequence, including sedimentological features, main compositional parameters (TIC = Total Inorganic Carbon, TOC = Total Organic Carbon, GS = Grain Size and mineralogical content (%), including: quartz (Qtz), chlorite (Chl), illite (Ill) and calcite (Cc)) and depositional subenvironments and/or process interpreted for each case.

<i>Comp depth (cm)</i>	<i>Unit</i>	<i>Laboratory code</i>	<i>Type of material</i>	<i>AMS ¹⁴C age (yr B.P.)</i>	<i>Corrected AMS ¹⁴C age</i>	<i>Calibrated corrected age (cal yrs BP) (2σ range)</i>
44,5	LC	D-AMS 001611	Bulk organic matter	5460 ± 35	-13 ± 35	<i>Modern</i>
123	LC	D-AMS 001114	Bulk organic matter	6537 ± 36	1064 ± 71	984 ± 187
197,7	LC	D-AMS 001113	Bulk organic matter	5441 ± 33	-32 ± 68	<i>Modern</i>
290,5	LC	D-AMS 001609	Bulk organic matter	6519 ± 31	1046 ± 66	979 ± 187
528,8	LC	D-AMS 001112	Bulk organic matter	6217 ± 52	744 ± 87	723 ± 179
627,2	LB	D-AMS 001111	Bulk organic matter	5743 ± 39	2718 ± 324	2808 ± 802
996,1	LA	D-AMS 001610	Bulk organic matter	7813 ± 40	4788 ± 325	5453 ± 824
1297,9	LA	D-AMS 001110	Bulk organic matter	9790 ± 54	6765 ± 339	7600 ± 580
1297,9	LA	ETH-45854	Charcoal	6765 ± 285	6765 ± 285	7600 ± 580

Table 2. Radiocarbon dates used for the construction of the age model for the Lake Banyoles sequence. A correction of 3025 ± 35 ¹⁴C years was applied to bulk sediment samples from units LA and LB, and 5473 ± 285 ¹⁴C years to uppermost lithological unit LC. Corrected dates were calibrated using CALIB 6.0 software and the INTCAL09 curve (Reimer et al., 2009); and the mid-point of 95.4% (2σ probability interval) was selected.

FIGURE CAPTIONS

Fig. 1. (A) Location of the Lake Banyoles within the Iberian Peninsula; (B) bathymetric map, basins and sub-basins (modified from Soler et al., 2009); (C) aerial photograph with seismic grids obtained with the Pinger 3.5 KhZ source (yellow) and Edgetech profiler (red), with indication of the seismic profile displayed below, long (dots) and short core (squares) locations; and (D) N-S seismic profile.

Fig. 2. (A) W-E seismic section (line 4) and correlation with core BAN-11-1A indicated by superposition of core image, sedimentological profile (see legend below) and density profile (g/cm^3); (B) S-N seismic section (line 24) with core BAN-11-1A location and limits of seismic units marked by blue dotted lines; (C) Location of (A) and (B) in the seismic grid.

Fig. 3. Composite sequence for Lake Banyoles record (core BAN-11-1A). From left to right: core image, sedimentary units, sedimentological profile (see legend in Fig. 2 and lithotypes description in Table 1), lightness record (L^*), magnetic susceptibility (MS) (SI units), total inorganic carbon (TIC), total organic carbon (TOC) (%), mineralogical composition (%), including: quartz (Qtz), chlorite (Chl), illite (Ill) and calcite (Cc) (see legend below); mean and mode grain size (μm) and grain size classes (sand, silt and clay) distribution (%) (see legend below). Homogenites and turbidite event layers are indicated by horizontal blue and orange bands, respectively.

Fig. 4: High resolution core images of the different lithotypes defined for the Lake Banyoles sequence: A, lithotype 1; B, lithotype 2; C, lithotype 3; D, lithotype 4; E,

alternation between lithotypes 1 and 4; F, turbidite sequence composed by lithotypes 6 (base) and 5 (mid-top of the core section); G, suspended sediments within sub-basin B1; and H, suspended sediments within sub-basin B2.

Fig. 5. Backscattered scanning electron images in selected intervals of cores BAN-11-1A, BAN-12-1 and 2. (A-C) Lithotype 1: (A) General view (3000x), (B) detail of endogenic carbonates (12000x), (C) detail of detrital grains and plant remains transported from the watershed (6000x). (D-F) Lithotype 4 (homogenites): (D) General view (3000x), (E) detail of a pyrite framboid (12000x), (F) detail of coccolithophorid remains transported from the calcareous bedrock of deepest sub-basin and reworked diatoms (12000x).

Fig. 6. (A) X-ray Fluorescence (XRF) scanner data of lithologic Unit LC. Element concentrations (Al, Si, Ti, Fe, Mn, Ca, Sr, S), expressed as counts per second, and Ti/Ca, Sr/Ca and Fe/Mn ratios are indicated. Core image, sedimentary units and sedimentological profile are also included (see legend in Fig. 2). Homogenites are indicated by horizontal blue bands. (B) Bipolar plot of Ca vs. Ti relationship along lithotypes 4 (homogenites), 1 and suspended sediments from short gravity cores BAN-11-1 and 2.

Fig. 7. (A) Chronological model of the composite sequence of Lake Banyoles, formed by long cores BAN-11-1A and short core 1A-1G, based on the linear interpolation of AMS ^{14}C dates (black and white dots) and 1963 AD maximum ^{137}Cs peak (star). Material used for dating and rejected dates are also indicated in the legend. Different models proposed for the uppermost part (1, 2 and 3) correspond to red, green and blue

lines, respectively. Homogenites and turbidite event layers are indicated by horizontal blue and orange bands, respectively. (B) ^{137}Cs and ^{210}Pb activity profiles for the uppermost 70 cm of the sequence. (C) Detail of age/depth relationships along the uppermost unit C.

Fig. 8. (A) Interpreted composite seismic profile between deepest sub-basins B1 and B2 with the location of short and long cores and interpreted deposits of homogenites derived from B1 (orange) and B2 (blue) sub-basins. (B) Correlation panel of short gravity cores (BAN-12-1, 2, 3, 4, 5, 6 and 8) and long core BAN-11-1A along a transect between sub-basins B1 and B2. Orange and blue-shaded areas represent correlation between homogenites derived from B1 and B2, respectively. (C) Core locations on the seismic grid in an aerial photograph of Lake Banyoles.

Figure 1
[Click here to download high resolution image](#)

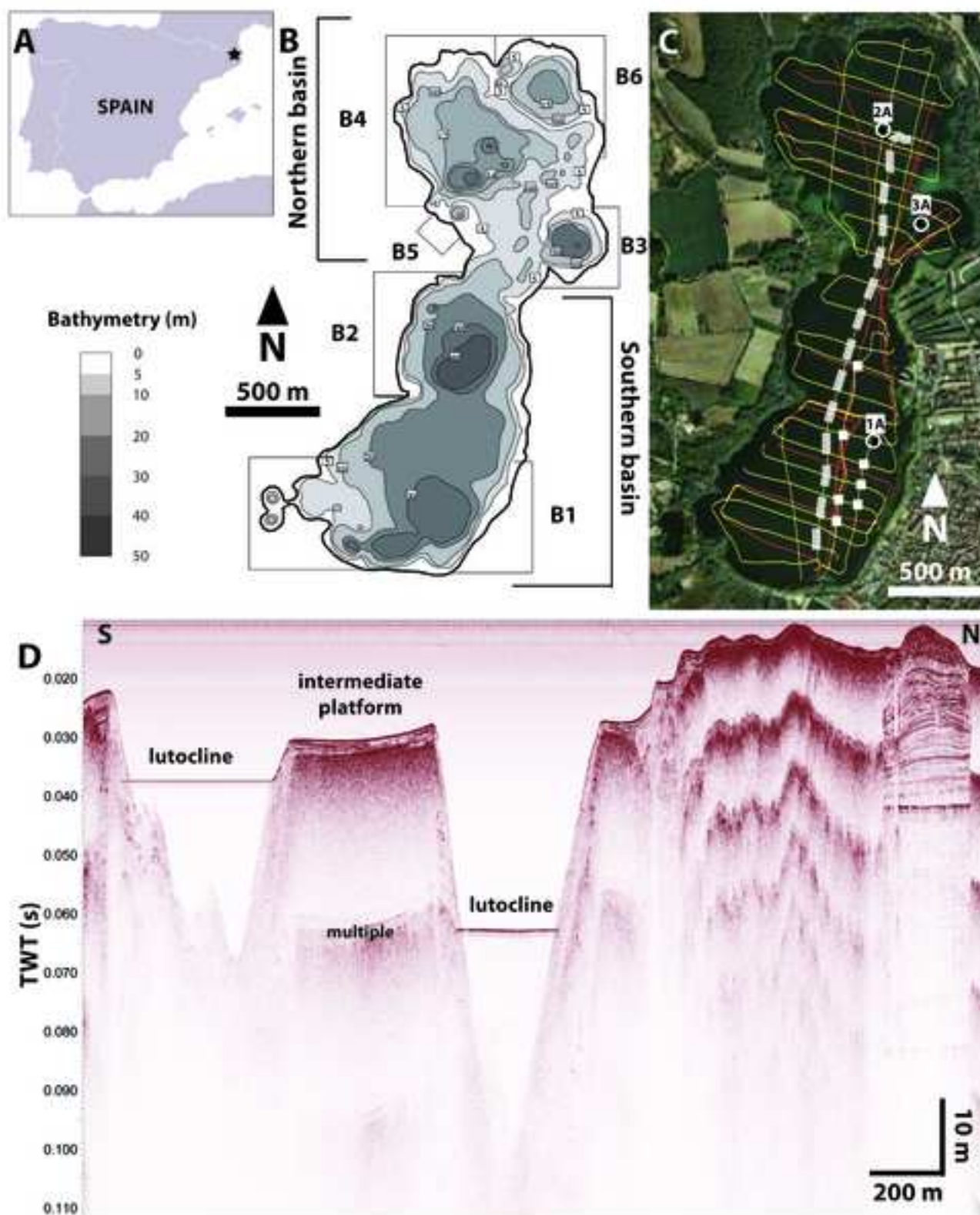


Figure 2
[Click here to download high resolution image](#)

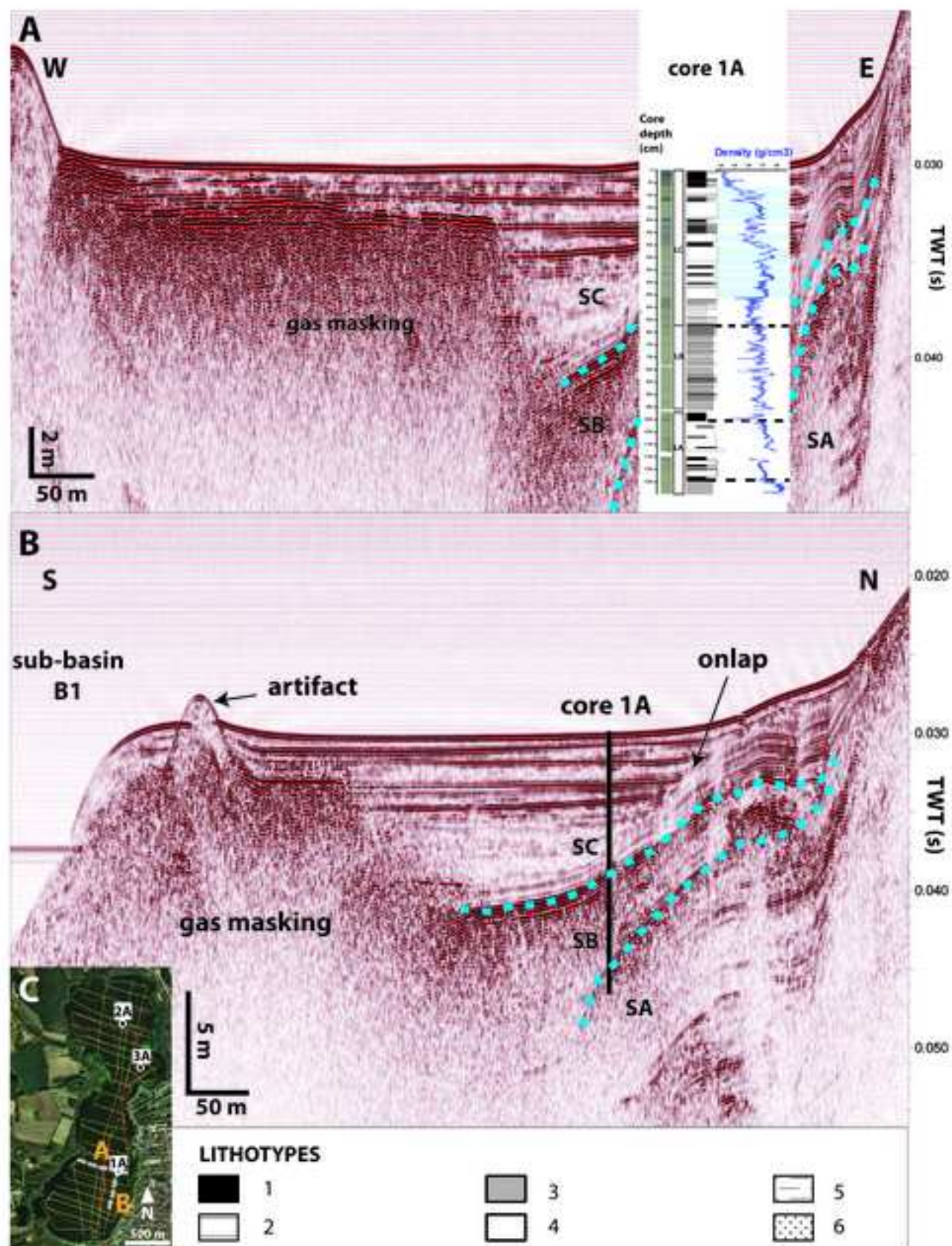


Figure 3
[Click here to download high resolution image](#)

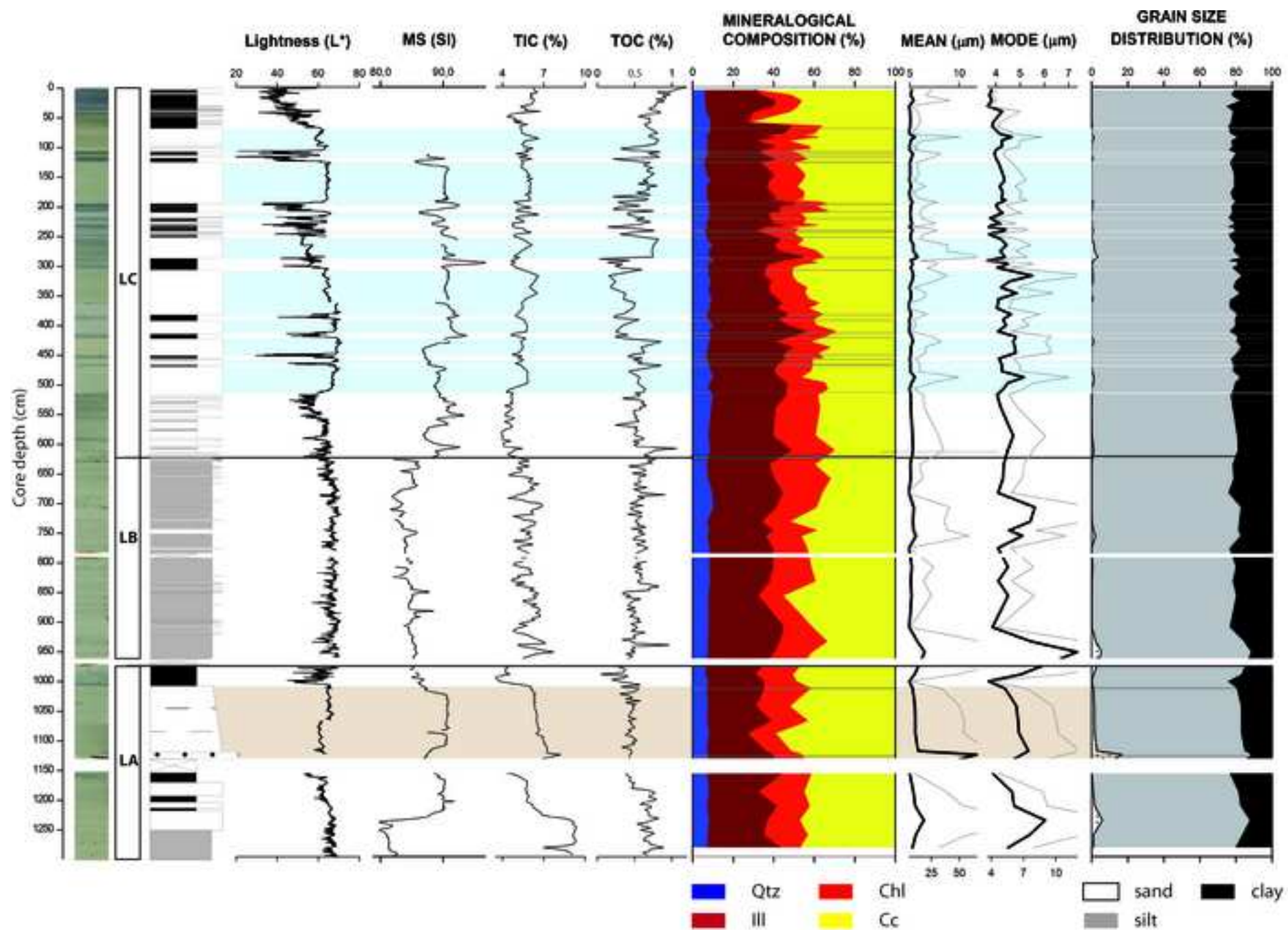


Figure 4
[Click here to download high resolution image](#)

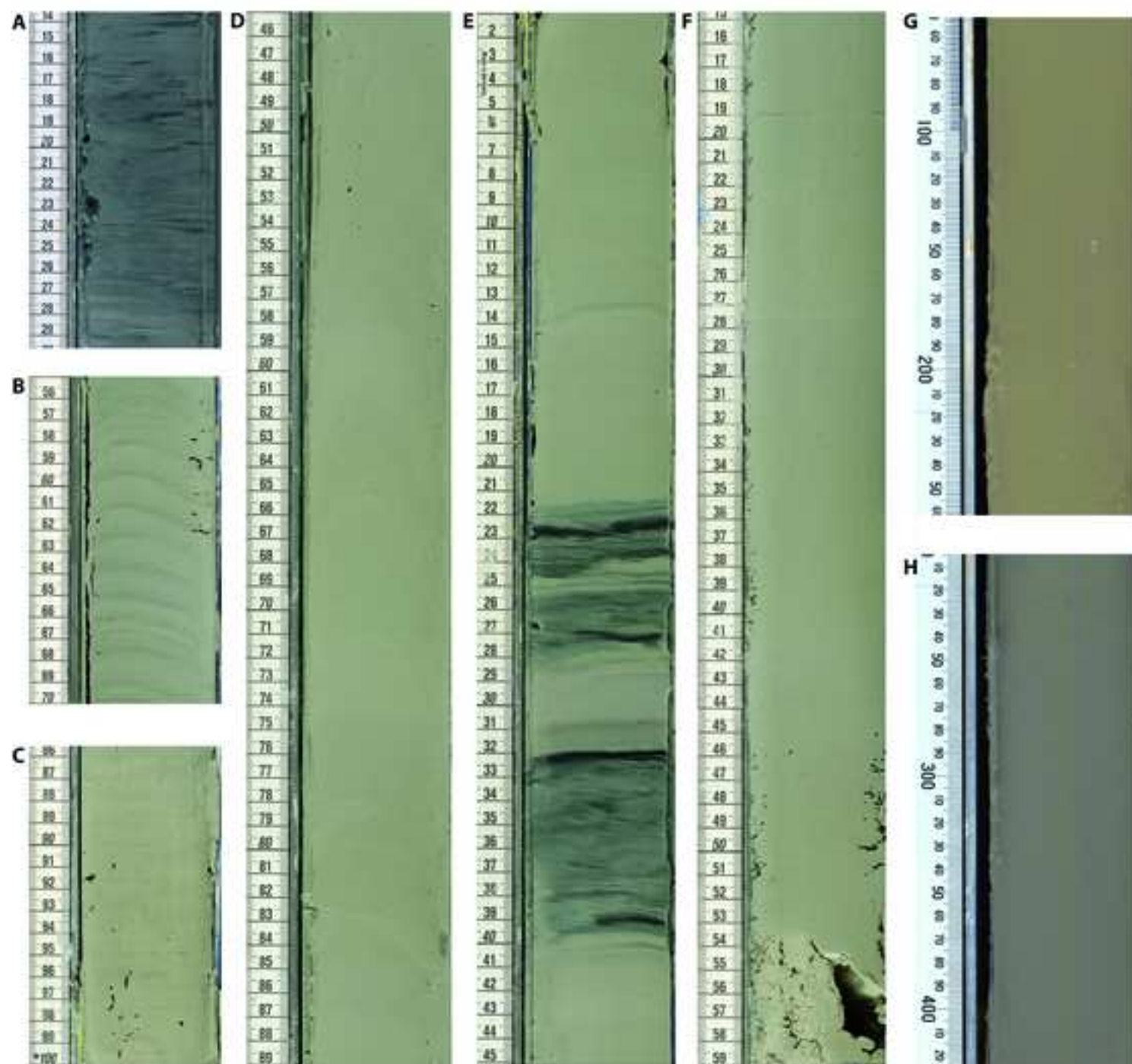


Figure 5
[Click here to download high resolution image](#)

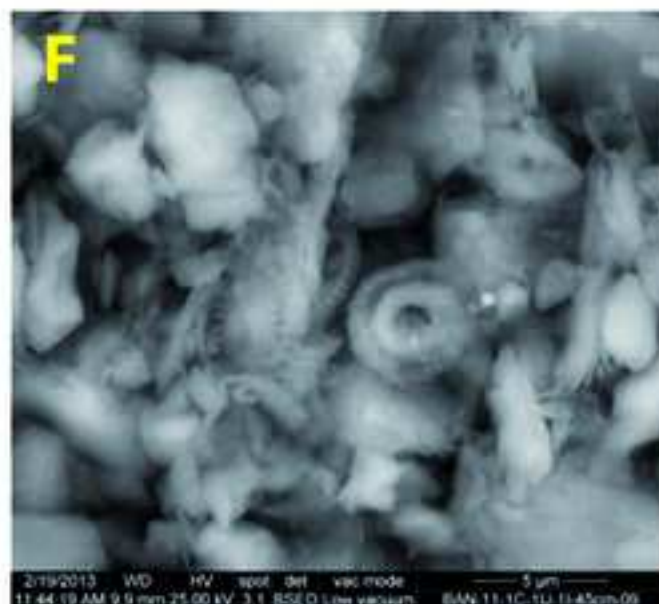
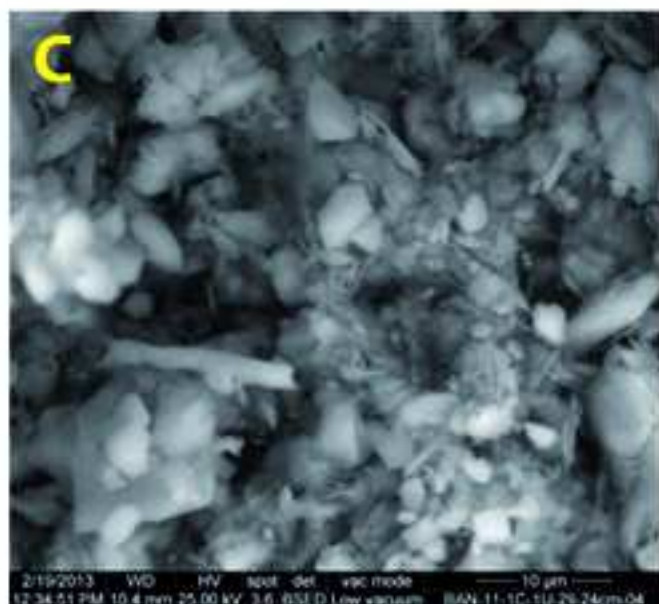
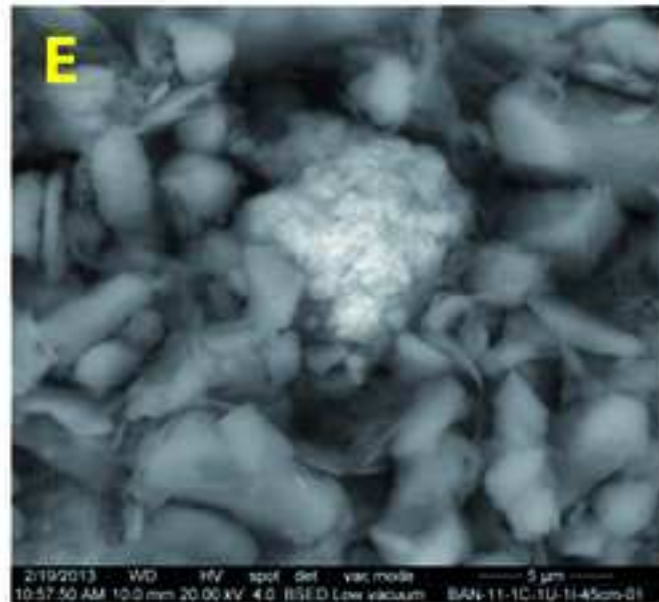
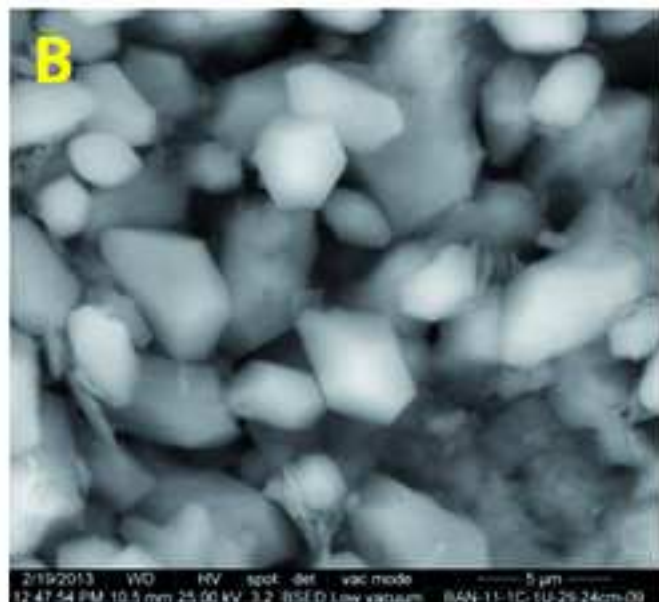
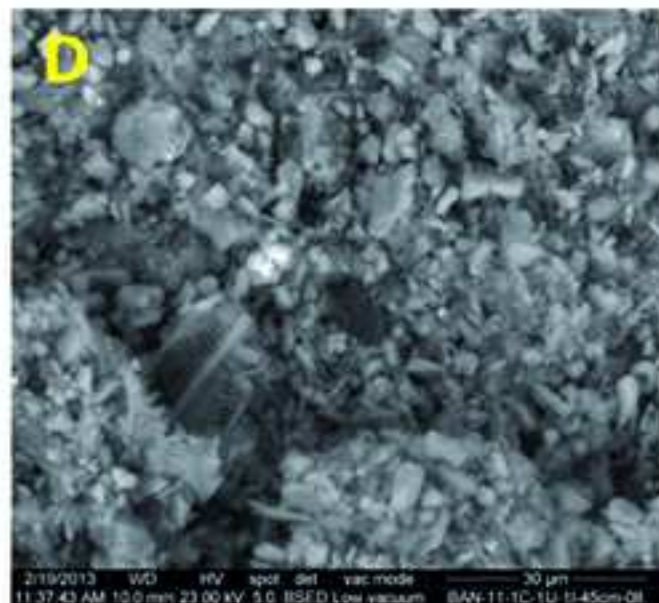
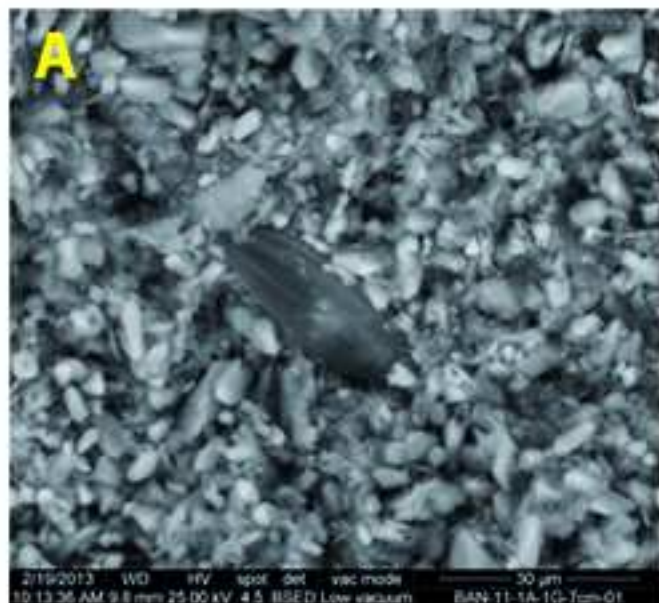


Figure 6
[Click here to download high resolution image](#)

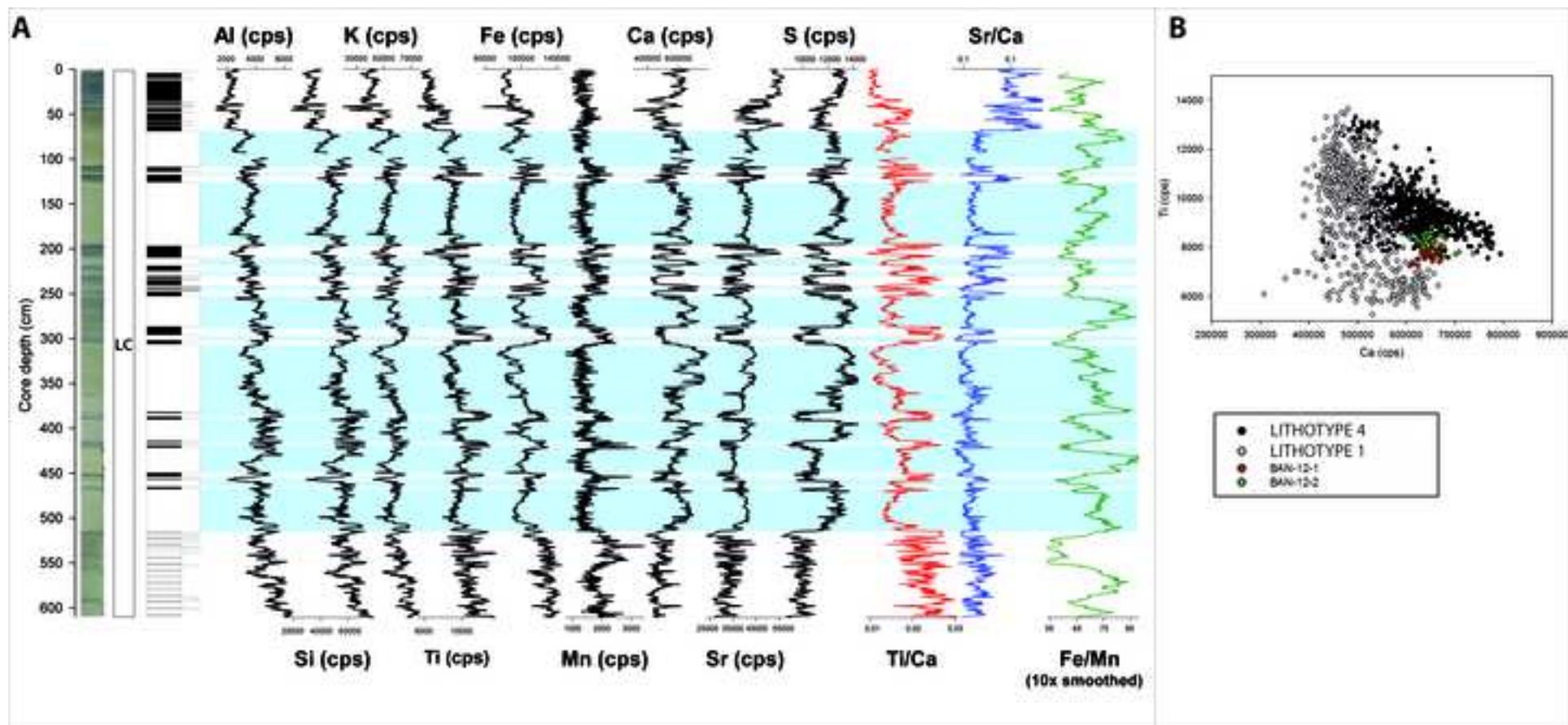


Figure 7
[Click here to download high resolution image](#)

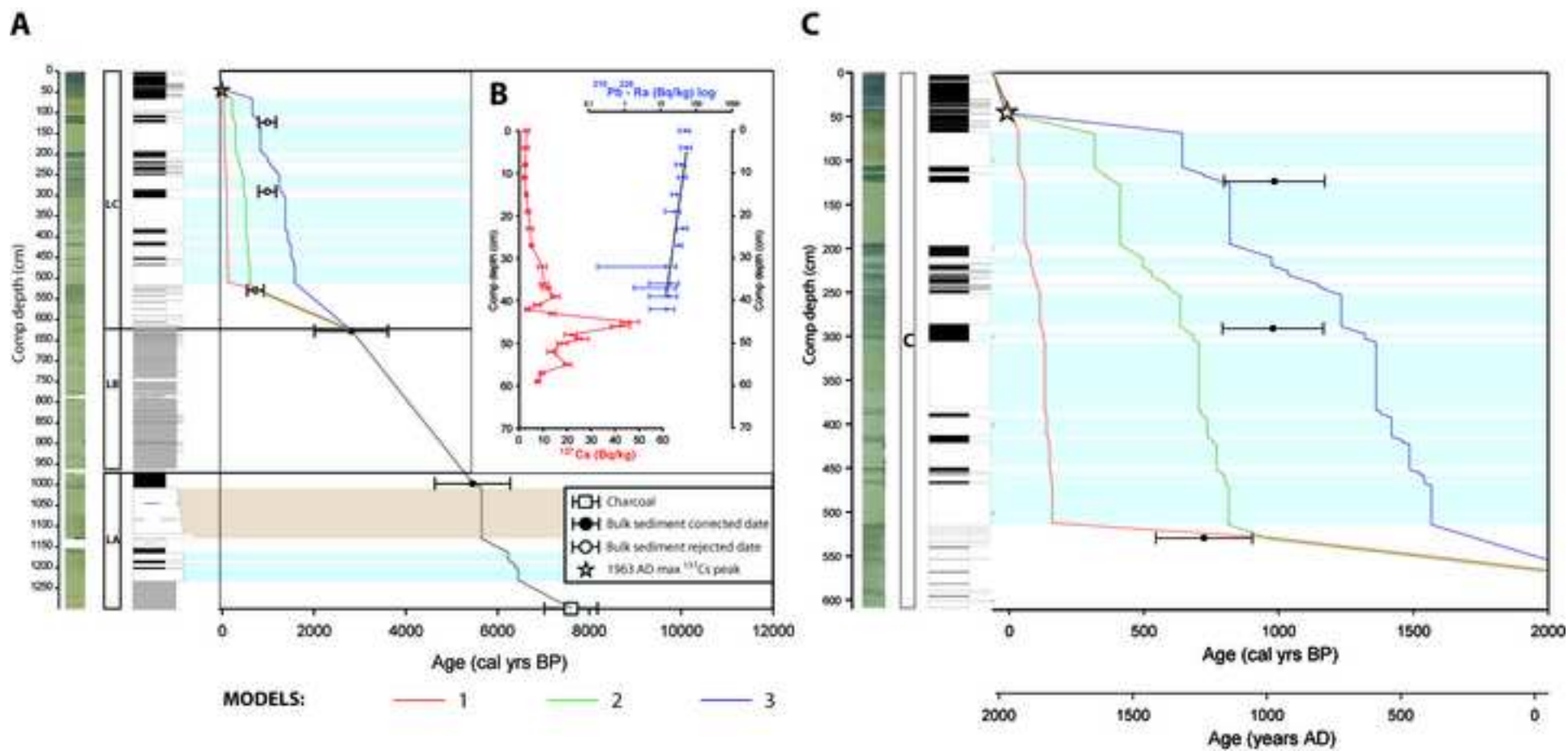


Figure 8
[Click here to download high resolution image](#)

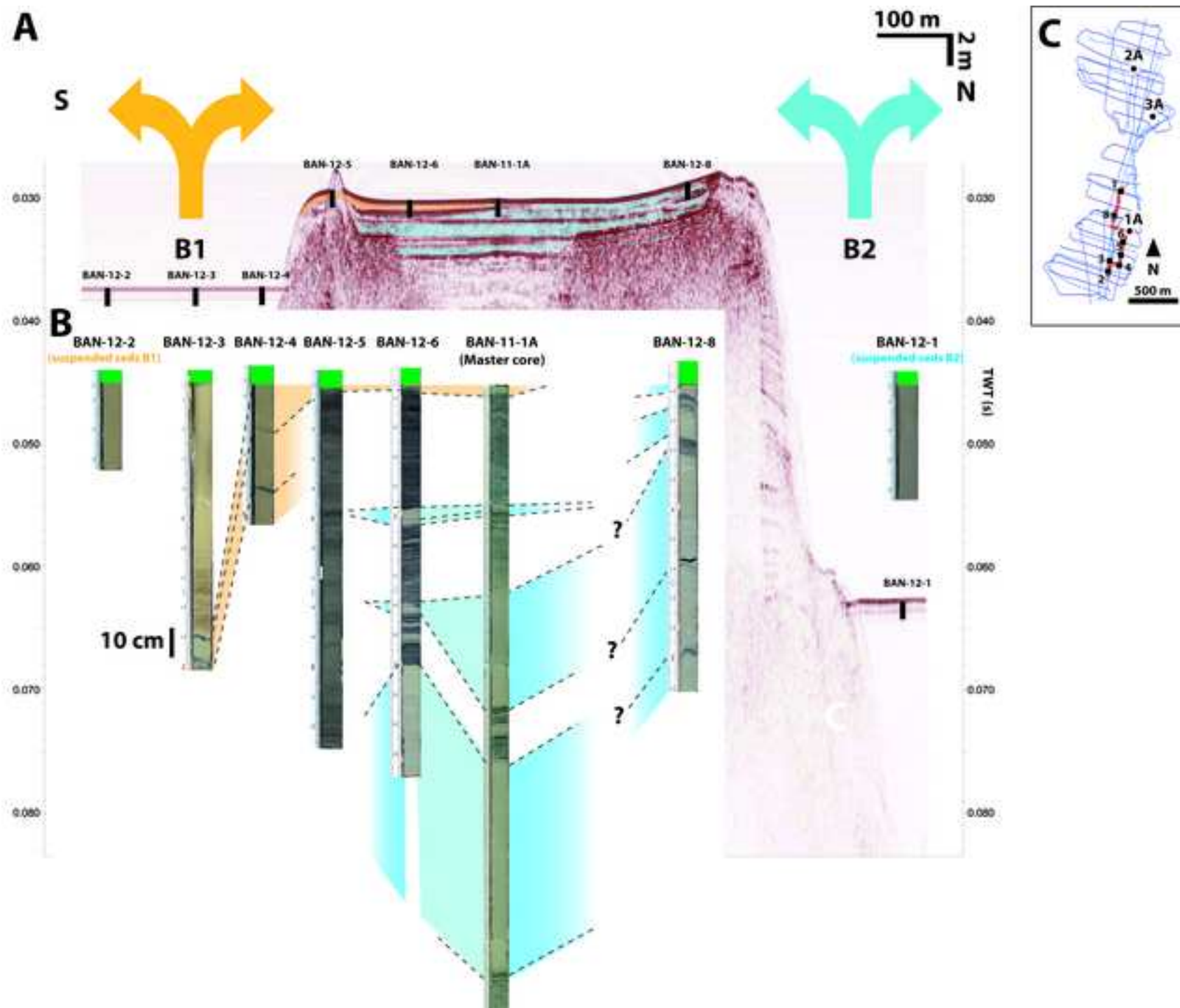


Table 1
Click here to download Table: table 1.docx

<i>Lithotype</i>	<i>Sedimentological features</i>	<i>Compositional parameters</i>	<i>Depositional subenvironment/ process</i>
<i>Banded and laminated</i>	1 <i>Dark-grey to black, massive to banded, carbonate-rich silts with diatoms</i> Fine grained carbonate mud composed by up to 10 µm hexagonal calcite grains with abundant to frequent ca. 50-60 µm reworked occasional reworked littoral carbonate-rich particles (ostracods, charophytes and carbonate coatings). Frequent ca. 25 µm detrital carbonate particles, plant remains and diatoms, locally abundant. Occasional quartz grains and < 20µm pyrite framboids.	TIC = 3.3% - 6.7 % TOC = 0.0% - 1.2 % Mean GS = 5 – 18 µm Mineralogy: Cc = 42.3%, Ill = 32.5%, Chl = 17.7%, Qtz = 7.4%	Deep, monomictic, occasionally anoxic brackish to freshwater lake with permanent, low-concentration turbidity plumes
	2 <i>Laminated fcs comprising alternating mm to 1 cm thick black and light-grey fine-grained silts</i> Black laminae: Fine-grained (up to 10 µm) hexagonal to sub-hexagonal calcite grains with abundant diatoms, up to 100 µm reworked littoral carbonate particles and frequent 20-30 µm detrital grains of quartz and carbonates. Light grey laminae: fine-grained, up to 10 µm irregular, reworked calcite crystals with frequent up to 40 µm clastic quartz and non-biogenic carbonates. Occasional to frequent up to 50 µm reworked littoral carbonate-rich particles.	TIC = 3.9 % – 6.2 % TOC = 0.2 %- 1.1 % Mean GS = 6.0 – 8.4 µm Mineralogy: Cc = 39.5%, Ill = 32.7%, Chl = 19.5%, Qtz = 8.2%	Relatively deep, carbonate-producing lake with seasonal anoxic hypolimnetic conditions
	3 <i>Grey, barely laminated to massive, carbonate-rich silts with evidences of bioturbation</i> 30-50 µm reworked biogenic carbonate particles with abundant up to 50 µm irregularly shaped detrital grains of quartz and carbonates. Frequent fine-grained, up to 10 µm calcitic mud.	TIC = 4.4% – 9.3% TOC = 0.3%- 1.0 % Mean GS =4.8 – 18.9 µm Mineralogy: Cc = 51.6%, Ill = 26.5%, Chl = 15.1%, Qtz = 6.9%	Shallow, carbonate-producing brackish lake with oxic conditions
<i>Massive</i>	4 <i>Light grey, massive fine-grained, carbonate-rich silts, occurring as mm to cm-thick intercalations or cm to dm-thick homogeneous layers</i> Up to 10 µm fine-grained irregularly-shaped calcite mud with abundant reworked diatoms. Frequent up to 50 µm reworked carbonate particles, sub-circular calcareous algae and pyrite framboids. Occasional plant remains.	TIC = 4.3% -6.8 % TOC = 0.1% - 0.9 % Mean GS = 5 – 12.6 µm Mineralogy: Cc = 44.7%, Ill = 31.7%, Chl = 16.2%, Qtz = 7.4%	Fluidization events and associated periodical and intense turbidity plumes

5	<i>Light grey/yellowish, massive, fine-grained, up to 1 m thick fining upwards sequences ranging from coarse to fine-grained silts</i> Dominant 10-15 µm reworked, sub-rounded to hexagonal calcite grains with reworked littoral carbonate-rich particles (up to 50-60 µm), more frequent towards the base.	TIC = 4.5 % - 7.3% TOC = 0.3 % - 0.6 % Mean GS = 8.2 – 13.0 µm Mineralogy: Cc = 40.9%, Ill = 32.7%, Chl = 18.8%, Qtz = 7.7%	Mass-wasting processes
6	<i>Light grey/yellowish, massive, fine-grained, carbonate-rich sands</i> 100-300 µm sub-rounded, biogenic, reworked carbonate particles with abundant up to 100 µm coarse, high relief detrital grains of quartz and non-biogenic carbonates. Abundant fine-grained matrix composed of up to 10 µm sub-rounded calcite crystals.	TIC = 7.2% - 8.8% TOC = 0.4% - 0.5 % Mean GS = 65.5 µm Mineralogy: Cc = 57.9%, Chl = 18.1%, Ill = 15.4%, Qtz = 8.6%	Mass-wasting processes

Table 1. Lithotypes defined for the Lake Banyoles sequence, including sedimentological features, main compositional parameters (TIC = Total Inorganic Carbon, TOC = Total Organic Carbon, GS = Grain Size and mineralogical content (%), including: quartz (Qtz), chlorite (Chl), illite (Ill) and calcite (Cc)) and depositional subenvironments and/or process interpreted for each case

Table 2
[Click here to download Table: table 2.docx](#)

<i>Comp depth (cm)</i>	<i>Unit</i>	<i>Laboratory code</i>	<i>Type of material</i>	<i>AMS ¹⁴C age (yr B.P.)</i>	<i>Corrected AMS ¹⁴C age</i>	<i>Calibrated corrected age (cal yrs BP) (2σ range)</i>
44,5	LC	D-AMS 001611	Bulk organic matter	5460 ± 35	-13 ± 35	<i>Modern</i>
123	LC	D-AMS 001114	Bulk organic matter	6537 ± 36	1064 ± 71	984 ± 187
197,7	LC	D-AMS 001113	Bulk organic matter	5441 ± 33	-32 ± 68	<i>Modern</i>
290,5	LC	D-AMS 001609	Bulk organic matter	6519 ± 31	1046 ± 66	979 ± 187
528,8	LC	D-AMS 001112	Bulk organic matter	6217 ± 52	744 ± 87	723 ± 179
627,2	LB	D-AMS 001111	Bulk organic matter	5743 ± 39	2718 ± 324	2808 ± 802
996,1	LA	D-AMS 001610	Bulk organic matter	7813 ± 40	4788 ± 325	5453 ± 824
1297,9	LA	D-AMS 001110	Bulk organic matter	9790 ± 54	6765 ± 339	7600 ± 580
1297,9	LA	ETH-45854	Charcoal	6765 ± 285	6765 ± 285	7600 ± 580

Table 2. Radiocarbon dates used for the construction of the age model for the Lake Banyoles sequence. A correction of 3025 ± 35 ¹⁴C years was applied to bulk sediment samples from units LA and LB, and 5473 ± 285 ¹⁴C years to uppermost lithological unit LC. Corrected dates were calibrated using CALIB 6.0 software and the INTCAL09 curve (Reimer et al., 2009); and the mid-point of 95.4% (2σ probability interval) was selected.